Electronic Supporting Information

for

A Metal–Organic Framework-Supported Dinuclear Iron Catalyst for Hydroboration of Carbonyl Compounds

Yi-Jie Zhu [a, b, c], Jun-Jie Wang [a], Jun-Yu Li [a, d], Teng Zhang *[a, c, d]

[a] State Key Laboratory of Structural Chemistry, Fujian Institute of Research on the Structure of Matter, Chinese Academy of Sciences, Fuzhou 350002, China

b College of Chemistry and Materials Science, Fujian Normal University, Fuzhou 350007, China

[c] Fujian College, University of the Chinese Academy of Sciences, Fuzhou 350002, China

[d] University of the Chinese Academy of Sciences, Beijing 100049, China

*Corresponding Author. Email: zhangteng@fjirsm.ac.cn

Table of Contents

1.General Information

All the experiments were performed under argon atmosphere inside the glovebox and Schlenk techniques unless otherwise indicated. All chemicals were commercially available and used without further purification. Tetrahydrofuran was dried with freshly activated 3 Å molecular sieves followed by distillation over Na/benzophenone and then stored inside the glovebox. ^{1}H and ^{13}C NMR spectra were recorded on a Bruker-BioSpin AVANCE III HD (400 MHz) or a JEOL ECZ600R (600 MHz) nuclear magnetic resonance spectrometer and referenced to the proton resonance resulting from incomplete deuteration of deuterated chloroform (δ 7.26) or deuterated dimethyl sulfoxide (δ 2.50). Inductively coupled plasma optical emission spectroscopy (ICP-OES) data were obtained with a HORIBA Jobin Yvon Ultima II with samples completely dissolved in HNO_3/HF diluent. Powder X-ray diffraction data were collected on a Rigaku Ultima IV powder diffractometer using Cu-Kα radiation (λ= 0.154 nm). UV-vis diffuse reflectance data were recorded under ambient conditions using a powder sample with $BaSO_4$ as a standard (100% reflectance) on a PerkinElmer Lamda-950 UV spectrophotometer and scanned in the range 200 - 1000 nm. Infrared spectra (IR) were recorded on a Bruker Vertex70 spectrometer as KBr pellets. The Raman spectra were collected on a Raman spectrometer (LabRAM HR Evolution) using 532 nm laser. Scanning electron microscopic (SEM) images and Energy dispersive spectroscopic (EDS) mapping data were obtained with a Phenom LE instrument. X-ray photoelectron spectroscopy (XPS) were performed on a Thermo Fisher ESCALAB 250Xi by using an Al Kα source (15 kV, 10 mA). Thermogravimetric analysis (TGA) was performed on Netzsch STA499F3 in a flowing nitrogen atmosphere with a heating rate of 10 °C/min with a range of 40-800 °C. Elemental analysis (C, H and N) was performed on a Vario EL Cube elemental analyzer.

2. Ligand Synthesis

2.1 Synthesis of 2-acetyl-5-methylpyridine (2).

Under nitrogen atmosphere, 2-bromo-5-methylpyridine (8.6 g, 50.0 mmol) was dissolved in 100 mL dry tetrahydrofuran. The solution was cooled to -78 °C and n-BuLi

(20 mL, 2.5 M in hexane) was added dropwise in 30 min. After stirred at -78°C for 90 min, 5 mL of dimethylacetamide was added into the system, which was allowed to react at -78°C to -50°C for another 10 hours. The reaction mixture was warmed to ambient temperature and saturated aqueous ammonium chloride (20 mL) was added to quench the reaction. The organic layer was separated, and the aqueous layer was extracted with tetrahydrofuran for several times. The combined organic layers were dried over anhydrous sodium sulfate, filtered, and concentrated under reduced pressure. The obtained liquid was further purified by column chromatography (EtOAc/CH_2Cl_2 = 1/9) to afford yellow oil product (6.19 g, yield: 91.60 %).^{1}H NMR (400 MHz, $CDCl_3$) δ 8.46 (s, 1H), 7.91 (d, J = 8.0 Hz, 1H), 7.58 (d, J = 8.0 Hz, 1H), 2.67 (s, 3H), 2.38 (s, 3H).

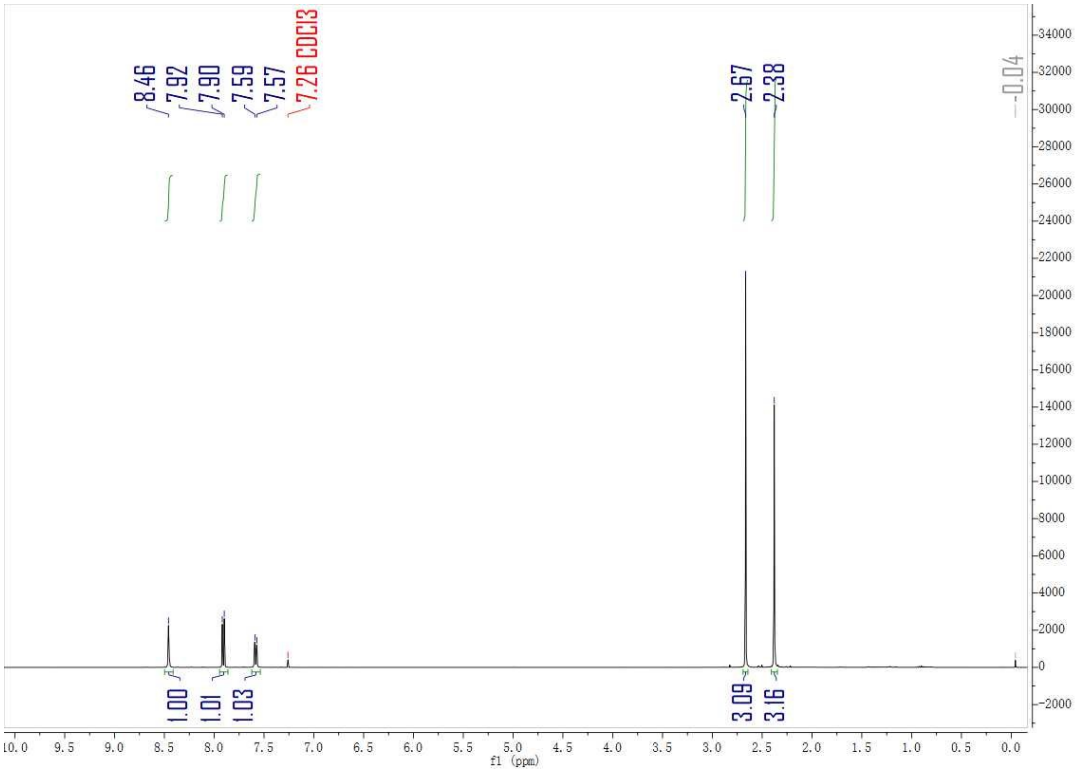

Figure S1. ^{1}H NMR (400 MHz, $CDCl_3$) spectrum of 2-acetyl-5-methylpyridine (**2**).

2.2 Synthesis of ethyl 5-methylpicolinate (4).

In a 250 mL round-bottom flask, 5-methylpyridine-2-carboxylic acid (5.0 g, 36.46 mmol) was dissolved in 100 mL dry ethanol. The mixture was heated to 60°C and concentrated sulfuric acid (6 mL) was added dropwise. The mixture was heated to reflux for another 18 hours. After cooling to ambient temperature, saturated $NaHCO_3$(aq) was added to the mixture until pH reached 7. The organic layer was

separated, and the aqueous layer was extracted with dichloromethane for several times. The combined organic layers were dried over anhydrous sodium sulfate, filtered, and concentrated under reduced pressure. The obtained liquid was further purified by column chromatography (EtOAc/CH_2Cl_2 = 1/4) to afford yellow oil product (4.90 g, yield: 81.24%). ^{1}H NMR (400 MHz, $CDCl_3$) δ 8.57 (s, 1H), 8.02 (d, J = 8.0 Hz, 1H), 7.62 (d, J = 8.0 Hz, 1H), 4.45 (q, J = 7.1 Hz, 2H), 2.40 (s, 3H), 1.42 (t, J = 7.1 Hz, 3H).

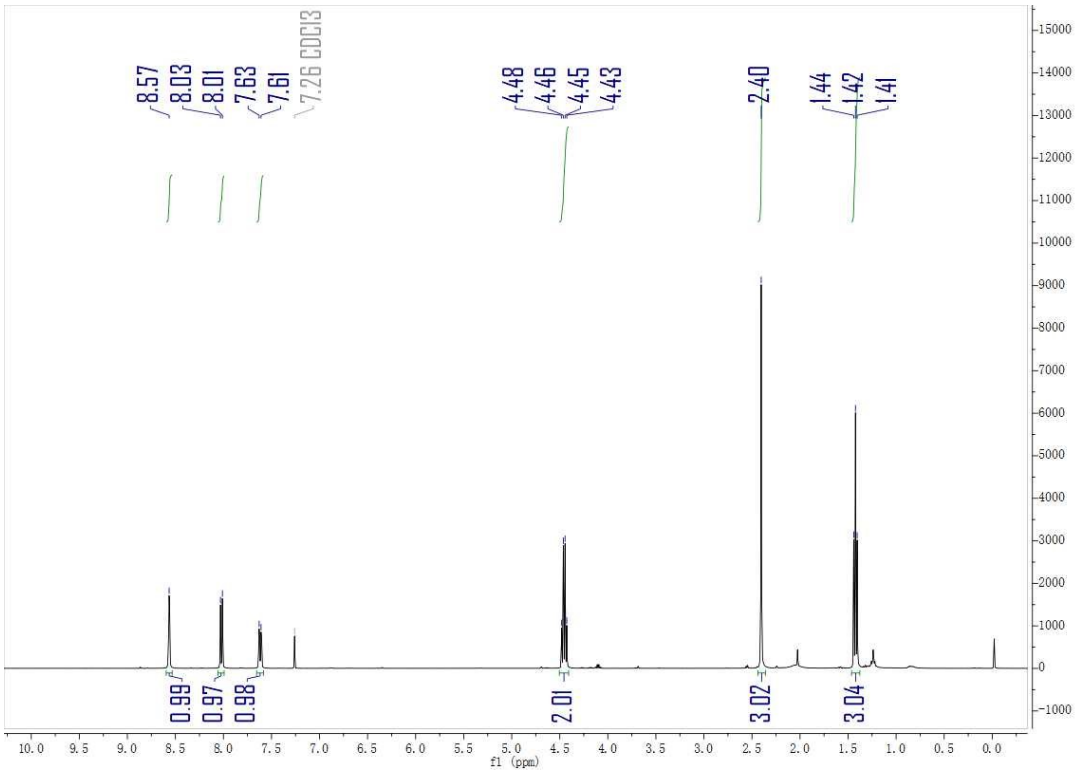

Figure S2. ^{1}H NMR (400 MHz, $CDCl_3$) spectrum of ethyl 5-methylpicolinate (**4**).

2.3 Synthesis of 1,3-bis(5-methyl-2-pyridyl)propan-1,3-dione (5).

Under nitrogen atmosphere, NaH (60% dispersion in mineral oil, 0.4615 g, 11.54 mmol) was suspended in dry tetrahydrofuran (50 mL) and the mixture was cooled to 0 °C. Then 5-acetyl-2-methylpyridine (1.1864 g, 8.78 mmol) was added gradually and stirred for 30 min at 0 °C. After that, ethyl 5-methylpicolinate (1.4558 g, 8.81 mmol) was added dropwise, and the reaction mixture was heated at 65 ℃ under reflux for 10 h. Subsequently, the solvent was removed under reduced pressure, and a solution of acetic acid/water mixture (v/v=1:5, 20.0 mL) was added to the viscous residue at 0 °C. After vigorously stirring, a yellow solid generated immediately and then was collected by suction filtration. The solid was washed with plenty of deionized water and dried in

vacuum at 70 °C to afford the crude product (1.0250 g, yield: 45.91%) and used in next step without further purification.

2.4 Synthesis of 3,5-bis(5-methyl-2-pyridyl)pyrazole (6).

Hydrazine monohydrate (80% in water, 3.1 ml) and 1,3-bis(5-methyl-2-pyridyl)propan-1,3-dione was dissolved in 50 ml of ethanol and refluxed for 12 h. After removal of the solvent by rotary evaporation, the resulting residue was washed with plenty of deionized water and dried in vacuum at 80 °C (0.93 g, yield: 92.08%). ^{1}H NMR (400 MHz, $CDCl_3$) δ 8.49 (s, 2H), 7.81 (d, J = 8.0 Hz, 2H), 7.58 (d, J = 8.1 Hz, 2H), 7.34 (s, 1H), 2.37 (s, 6H). ^{13}C NMR (101 MHz, $CDCl_3$) δ 149.73, 137.70, 132.57, 119.92, 101.24, 18.53.

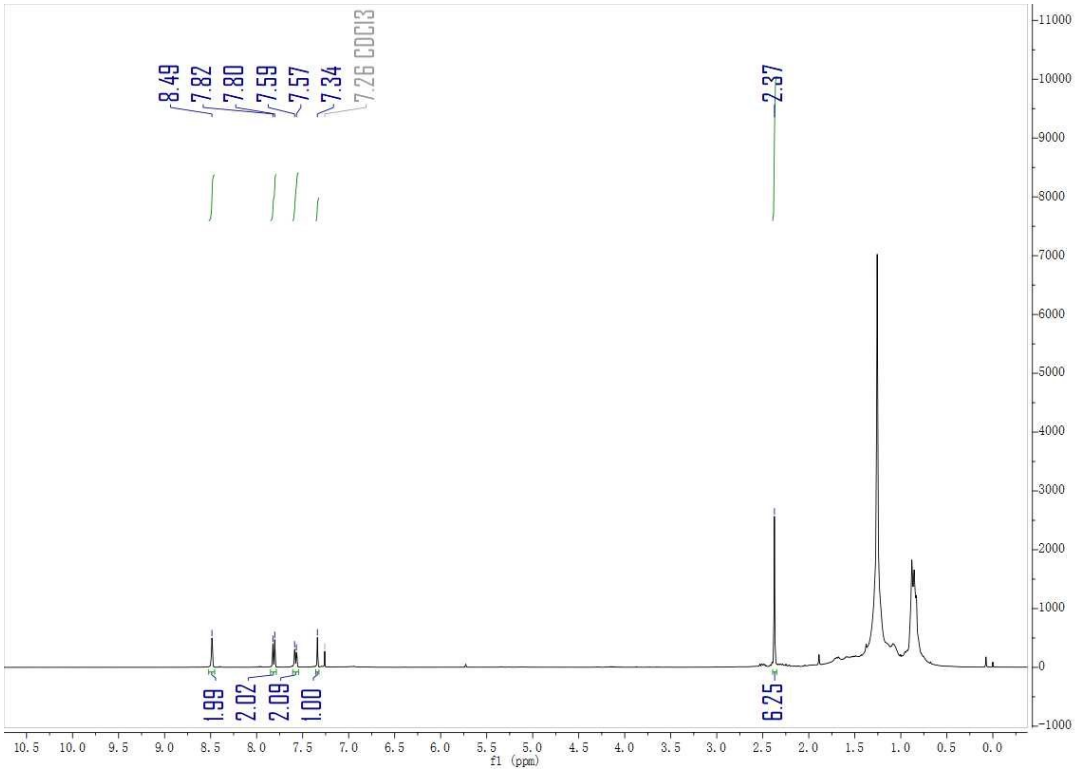

Figure S3. ^{1}H NMR (400 MHz, $CDCl_3$) spectrum of 3,5-bis(5-methyl-2-pyridyl)pyrazole (**6**).

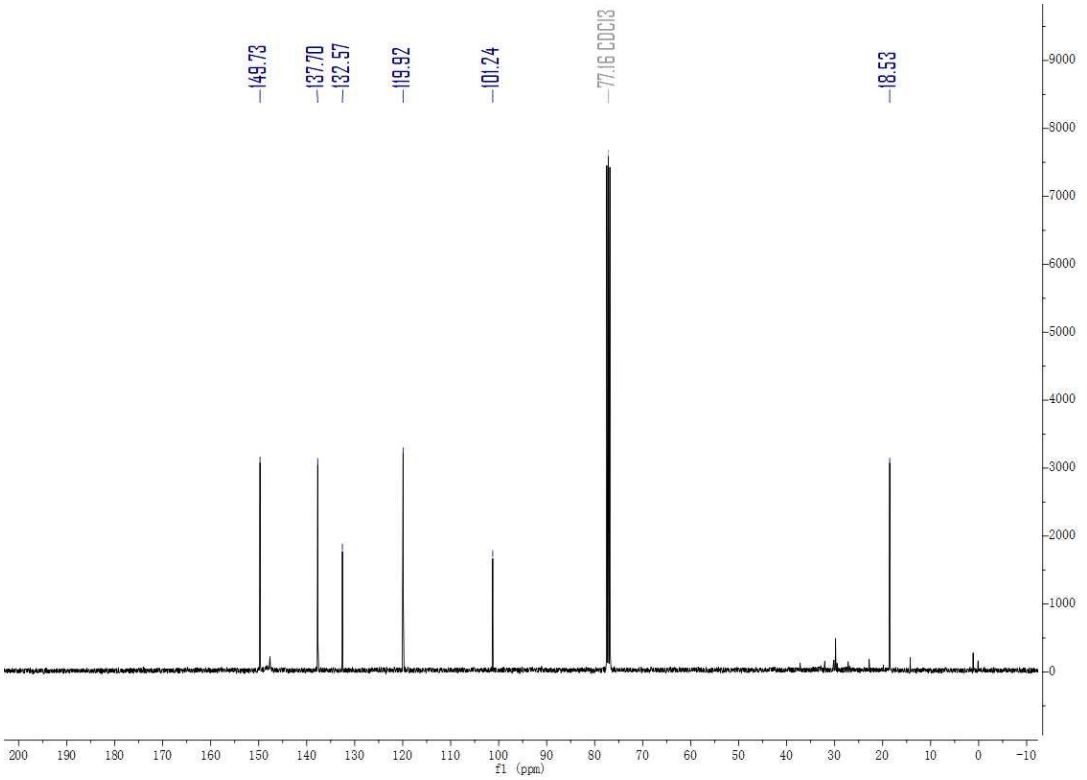

Figure S4. ^{13}C NMR (101 MHz, $CDCl_3$) spectrum of 3,5-bis(5-methyl-2-pyridyl)pyrazole (**6**).

2.5 Synthesis of 3,5-bis(5-carboxy-2-pyridyl)pyrazole (H_3bppz, 7).

3,5-bis(5-methyl-2-pyridyl)pyrazole (0.5 g, 2.0 mmol) was added to a solution of $KMnO_4$ (1.2628 g, 8.0 mmol) in 100 ml of deionized water and the mixture was refluxed for 6 h. After all of the potassium permanganate had been consumed, the dark brown mixture was filtered while hot. The supernatant was then slowly acidified with 1 M HCl to obtain a small amount of while precipitate at pH to 1-2. The mixture was left to stand overnight at 0 ℃ to obtain large quantities of white precipitate, which was collected by filtration, washed with large amount of deionized water and dried in vacuum at 100 °C as the product (0.16 g, yield: 25.81%). ^1H NMR (400 MHz, DMSO-d_6) δ 13.45 (s, 2H), 9.13 – 9.10 (m, 2H), 8.35 (d, J = 10.4 Hz, 2H), 8.14 (d, J = 8.2 Hz, 2H), 7.69 (s, 1H). ^{13}C NMR (101 MHz, DMSO-d_6) δ 166.22, 150.44, 138.24, 125.44, 119.66, 104.26. Elemental analysis (%): calc. for $C_{15}H_{10}N_4O_4$: C 58.06, H 3.26, N 18.06; found.: C 56.63, H 3.68, N 18.12.

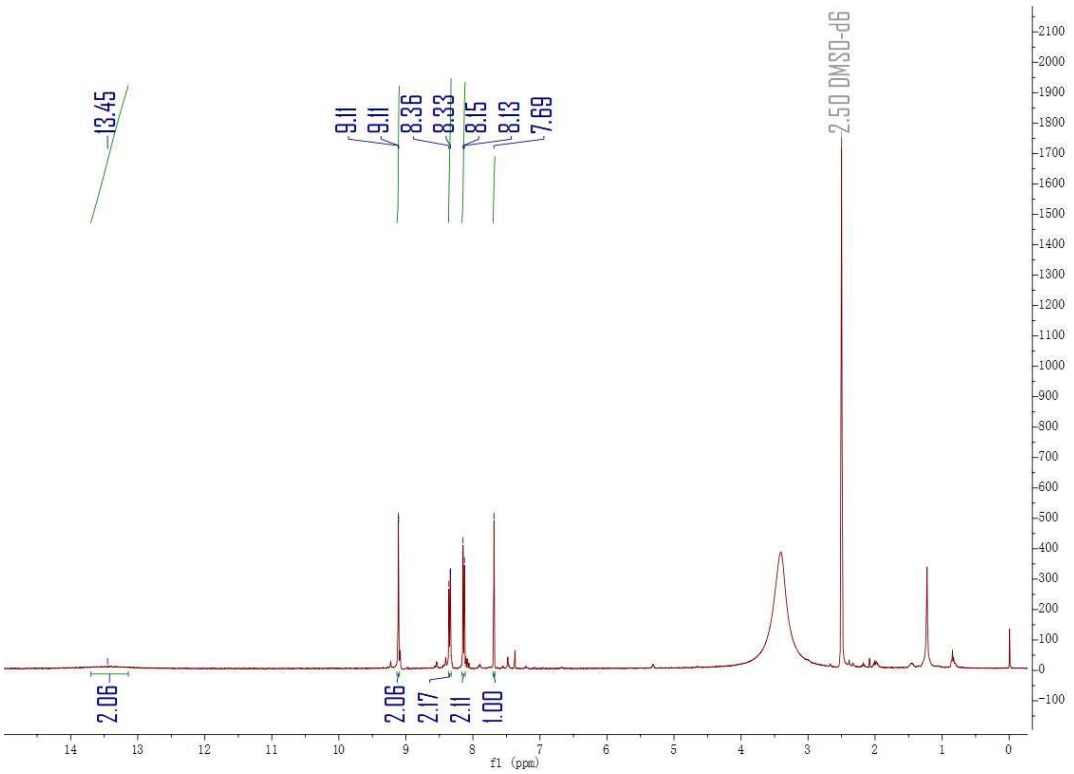

Figure S5. ^{1}H NMR (400 MHz, DMSO-d_6) spectrum of 3,5-bis(5-carboxy-2-pyridyl)pyrazole (H_3bppz, **7**).

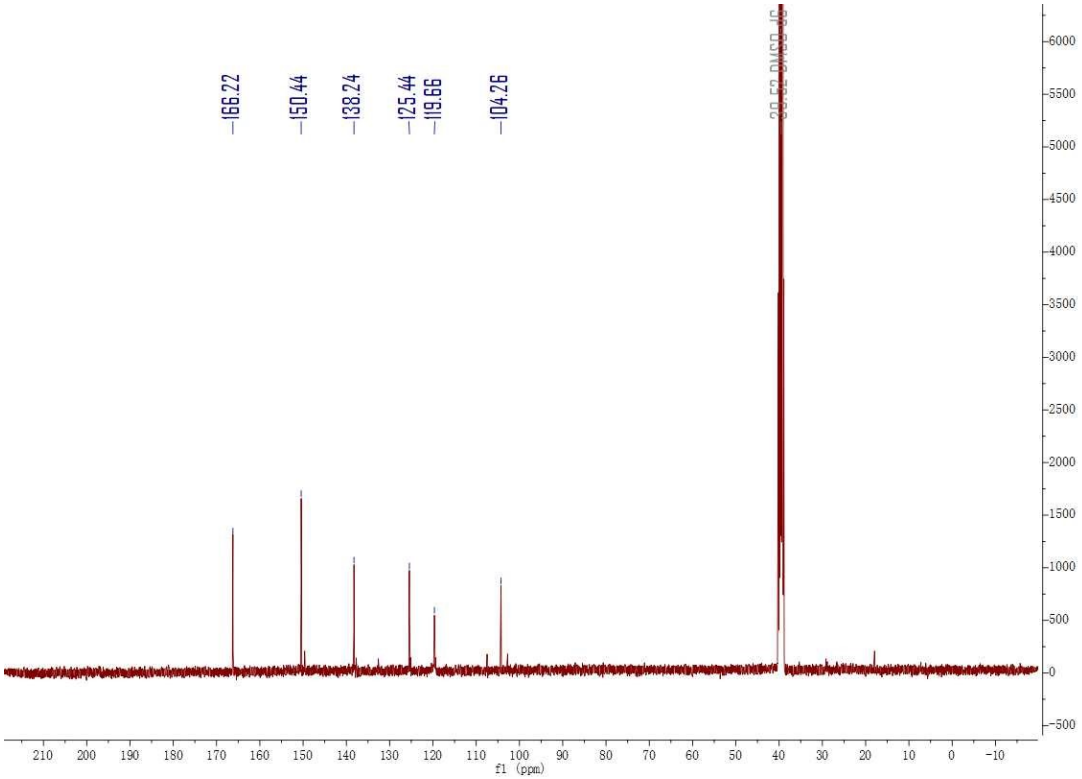

Figure S6. ^{13}C NMR (101 MHz, DMSO-d_6) spectrum of 3,5-bis(5-carboxy-2-

pyridyl)pyrazole (H_3bppz, **7**).

3. Crystallographic Information and Additional Structural Figures

Single crystal X-ray diffraction of FICN-7 was performed with a Bruker D8 Venture equipped with Mo-Kα radiation (λ = 0.71073 Å) at 150 K. The frames were integrated with the Bruker SAINT© build in APEX II software package using a narrow-frame integration algorithm, which also corrects for the Lorentz and polarization effects. Absorption corrections were applied using SADABS. Structures were solved by intrinsic phasing and refined to convergence by least squares method on F^2 using the SHELX-2019 software suite. All non-hydrogen atoms are refined anisotropically. Scattering from the highly disorder guest molecules were modelled by the SQUEEZE program in PLATON software suite.[1-2] A solvent mask was calculated and 1898 electrons were found in a volume of 8056Å^3 in 1 void per unit cell. This is consistent with the presence of 24 DMF[C3H7NO] solvent molecules per Formula Unit or 48 DMF molecules per unit cell which account for 1920 electrons per unit cell.

Table S1. Crystallographic information of FICN-7.

Name	FICN-7
Formula	$C_{60}H_{48}N_{16}O_{32}Zr_6 \cdot 24C_3H_7NO$
Formula weight	3806.76
Temperature (K)	150.03
Crystal system	orthorhombic
Space group	*Pnnm*
a, Å	31.786(3)
b, Å	13.9537(15)
c, Å	24.406(2)
α, °	90
β, °	90
γ, °	90
Volume (Å^3)	10824.8(18)
Z	2
Density (calc. g/cm^3)	1.168

Absorption coeff. (mm^{-1})	0.352
F(000)	3952
2θ range for data collection/°	5.108 - 46.512
Index ranges	-34 ≤ h ≤ 35, -15 ≤ k ≤ 15, -24 ≤ l ≤ 27
Reflections collected	35104
Independent reflections	7973 [Rint = 0.1434, Rsigma = 0.1067]
Data/restraints/parameters	7973/36/240
Goodness-of-fit on F^2	0.990
Final R indexes [I>=2σ (I)]	R1 = 0.0688, wR2 = 0.1902
Final R indexes [all data]	R1 = 0.1009, wR2 = 0.2117
Largest diff. peak/hole / e $Å^{-3}$	0.57/-0.96

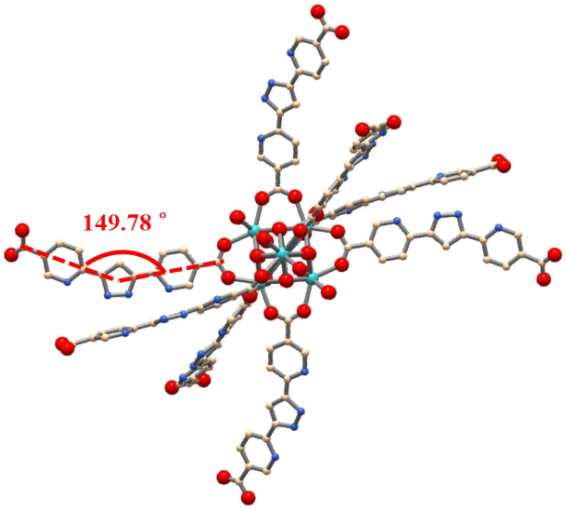

Figure S7. Structure of $Hbppz^{2-}$ linkers and the Zr_6O_8 inorganic nodes in FICN-7 as determined by analysis of single-crystal X-ray diffraction data. Cyan, red, blue, and beige spheres represent Zr, O, N, and C atoms, respectively; H atoms are omitted for clarity.

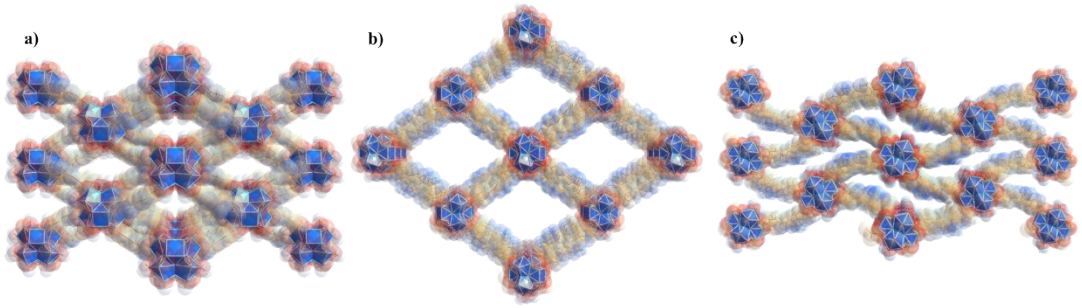

Figure S8. Space-filling model of FICN-7 viewed along a) [100]; b) [010] and c) [001] directions.

Table S2. Fraction atomic coordinates for the structure model of solvated FICN-7.

Atomic number	X	Y	Z
Zr1	0.48976	0.42018	0.42474
O2	0.61516	0.52569	0.55467
O3	0.59975	0.41026	0.44412
O4	0.42778	0.39890	0.39030
O5	0.47719	0.32115	0.43121
O6	0.53725	0.48908	0.57929
O7	0.54312	0.37036	0.39262
C8	0.58307	0.37273	0.40483
C9	0.61082	0.57072	0.59370
O10	0.48970	0.42717	0.33126
H11	0.06010	0.22682	-0.16743
C12	0.11948	0.25795	-0.19826
C14	0.16236	0.25197	-0.19859
C15	0.18124	0.20443	-0.16309
H16	0.21524	0.19829	-0.16203
C17	0.15563	0.16405	-0.12849
H18	0.17044	0.12717	-0.10167
C19	0.11133	0.17076	-0.12948

C20	0.09398	0.21937	-0.16532
C21	0.18916	-0.06466	-0.11409
H22	0.19224	-0.02533	-0.08295
C23	0.22436	-0.08602	-0.14279
C25	0.22331	-0.13521	-0.18264
C26	0.18450	-0.16515	-0.19488
H27	0.18234	-0.20434	-0.22627
C28	0.14783	-0.14409	-0.16598
H29	0.11815	-0.16780	-0.17587
C30	0.14961	-0.09330	-0.12483
N31	-0.33016	0.15604	0.23146
N32	-0.30061	0.12643	0.20018
C33	-0.26332	0.15545	0.21136
C34	-0.26955	0.20549	0.25142
C35	-0.31271	0.20420	0.26301
H36	-0.36212	0.14319	0.23069
H38	-0.24627	0.23856	0.26881
Zr39	0.57104	0.47873	0.50000
O40	0.52645	0.40460	0.50000
O41	0.54816	0.57275	0.50000

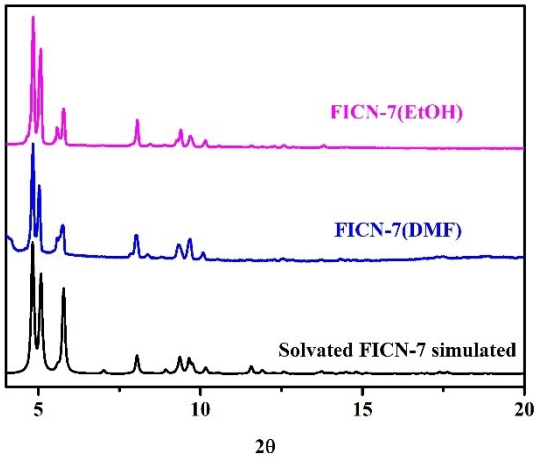

Figure S9. Experimental PXRD patterns of **FICN-7(DMF)** (blue) and **FICN-7(EtOH)**

(pink) as well as simulated pattern from the solvated **FICN-7** (black).

4. Additional Characterization Data of FICN-7 and Metalated FICN-7

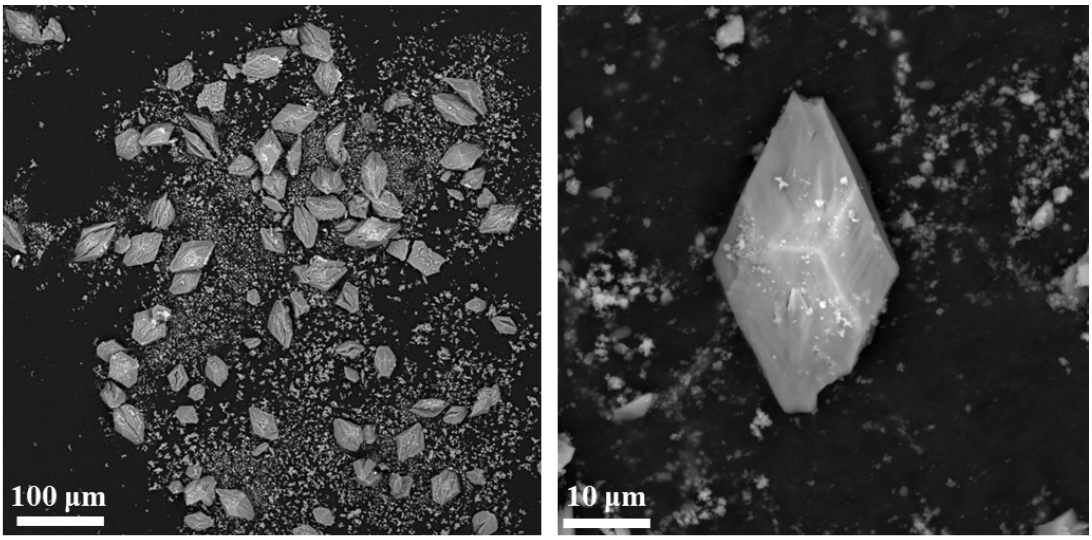

Figure S10. SEM images of FICN-7.

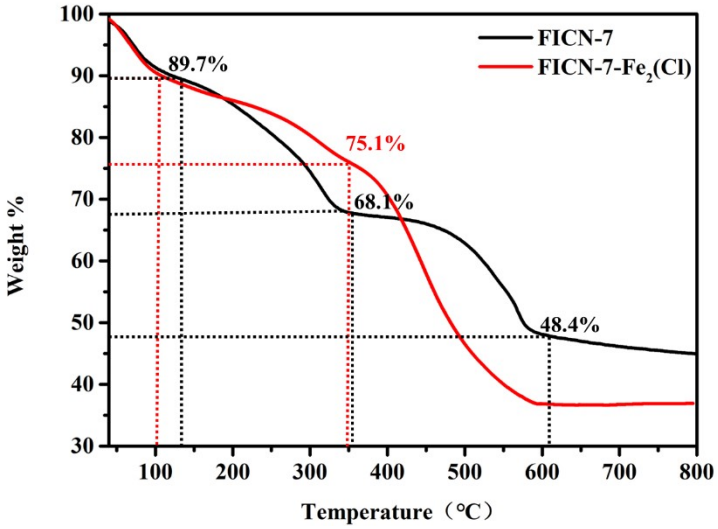

Figure S11. Thermogravimetric analysis (TGA) curve of FICN-7 and FICN-7-Fe_2(Cl) tested at 10 ºC/min in N_2 atmosphere.

Table S3. ICP-OES analysis of FICN-7-Fe_1 (Cl) and FICN-7-Fe_2 (Cl).

	ICP-OES	Metal Loading
FICN-7-Fe_1(Cl)	Zr 18.24% Fe 6.63%	44%
FICN-7-Fe_2(Cl)	Zr 16.82% Fe 9.41%	68%

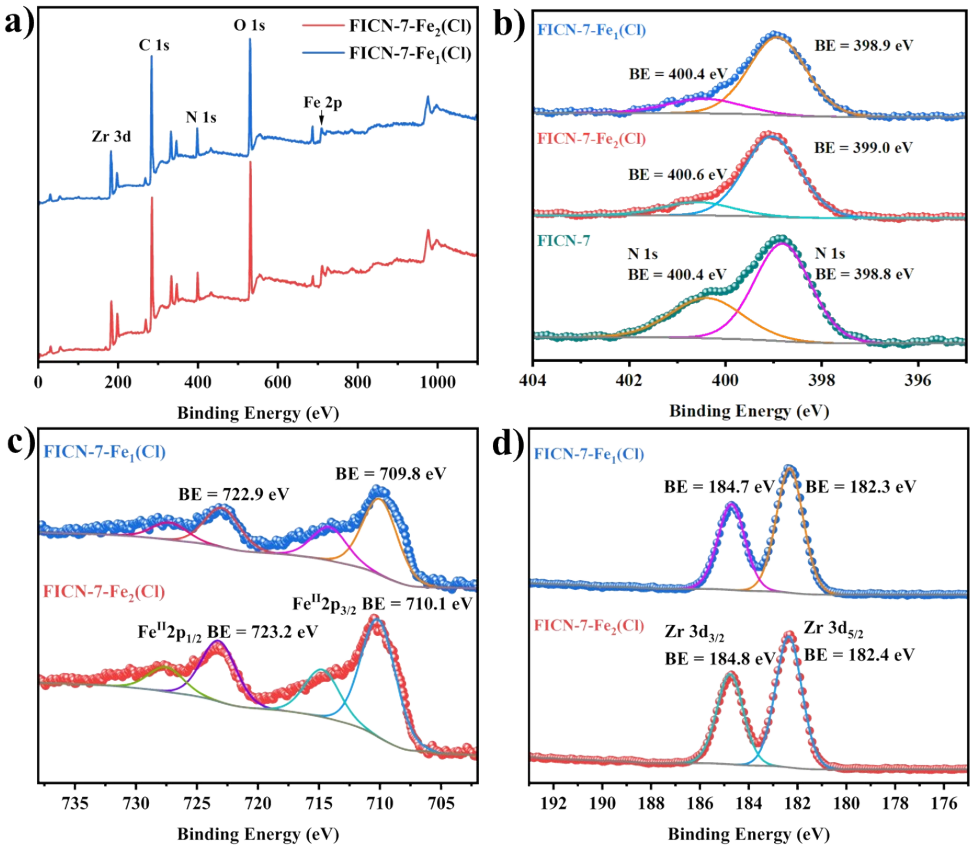

Figure S12. XPS spectra of FICN-7, FICN-7-Fe_2(Cl) and FICN-7-Fe_1(Cl).

5 XAS Analysis

The Fe K-edge XAS spectra were collected at beamline BL14W1 of Shanghai Synchrotron Radiation Facility (SSRF), China. Data were processed using the Athena and Artemis programs of the Demeter package based on FEFF 6.[3-4] Fits were performed with a *k*-weight of 2 in *R*-space. Refinement was performed by optimizing an amplitude factor S_0^2 and energy shift ΔE_0 which are common to all paths, in addition to parameters for bond length (ΔR) and Debye-Waller factor (σ^2). A universal S_0^2 was used for the fitting of FICN-7-Fe_2(Cl) and FICN-7-Fe_1(Cl), while other parameters are fitted separately for each sample.

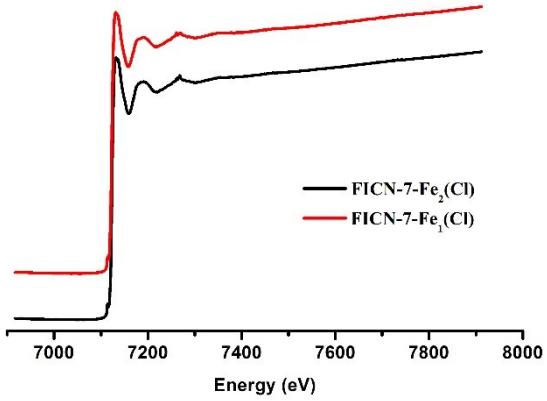

Figure S13. Normalized Fe K-edge XAS spectra for FICN-7-Fe_2(Cl) (black) and FICN-7-Fe_1(Cl) (red).

Table S4. Summary of EXAFS fitting parameters of FICN-7-Fe_2(Cl) and FICN-7-Fe_1(Cl).

Sample	FICN-7-Fe_2(Cl)	FICN-7-Fe_1(Cl)
Fitting range	k 3.00 – 12.391 Å^{-1} R 1.2 – 2.5 Å	k 3.00 – 12.395 Å^{-1} R 1.2 – 2.5 Å
Independent points	14	
Variables	11	
R-factor	2.7%	3.7%
S_0^2	0.771±0.236	
ΔE_0(eV)	4.36±4.47	7.21±5.38
N (Fe-N)	2	2
R (Fe-N) (Å)	2.01±0.05	2.04±0.05
σ^2 (Fe-N) (Å^2)	0.0035±0.0056	0.0024±0.0054
N (Fe-Cl)	1.5	1
R (Fe-Cl) (Å)	2.27±0.03	2.29±0.04
σ^2 (Fe-Cl) (Å^2)	0.0045±0.0042	0.0029±0.0050

6. Catalytic Hydroboration of Carbonyl Compounds

6.1 Catalyst heterogeneity test.

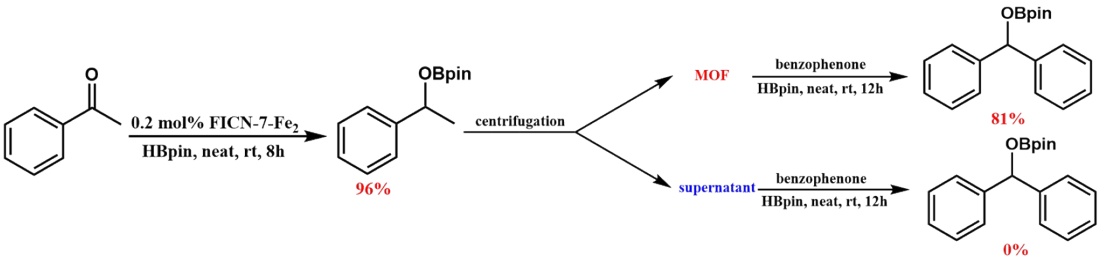

Scheme S1. Schematic representation of the heterogeneity test experiment.

After the completion of a standard catalysis experiment (0.2 mol% Fe, 8 h), FICN-7-Fe_2 catalyst was separated from the supernatant via centrifugation, and the solid and supernatant were placed in two different vials separately. HBpin (377 µL, 2.6 mmol) and benzophenone (0.364 g, 2.0 mmol) was added to each of the portions. The mixture was stirred for 12 h at room temperature and yield of the product was determined by ^{1}H NMR as described in Section 5.1. A yield of 81% was observed in the hydroboration of ketones catalyzed by FICN-7-Fe_2 while 0% yield was observed in the reaction done with the supernatant liquid. These two experiments confirm the heterogeneity of FICN-7-Fe_2 in the hydroboration of ketones.

6.2 Recyclability test.

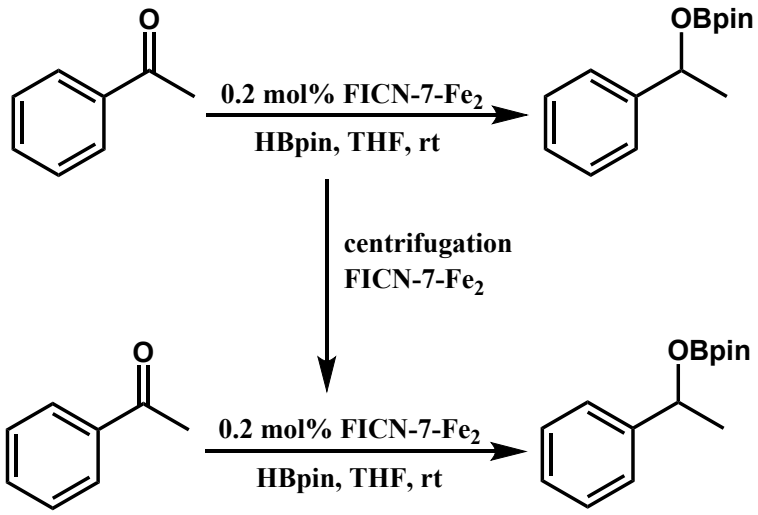

Scheme S2. Recycle and reuse of FICN-7-Fe_2 for hydroboration of acetophenone.

After the completion of a standard catalysis experiment (0.2 mol% Fe), FICN-7-Fe_2 catalyst was centrifuged out of suspension and transferred to another vial with HBpin (754 µL, 5.2 mmol) and acetophenone (467 µL, 4.0 mmol). The reaction was run for

another certain amount of time at room temperature with slow stirring. The reaction was then worked up with the procedure described in Section 5.1 and the yield of the product was determined by ^{1}H NMR.

Table S5. Time, conversion and yields for the recycling test of FICN-7-Fe_2 MOF.

No. of Run	Time (h)	Conversion (%)	NMR yield (%)
Run-1	2	98	95
Run-2	6	88	81
Run-3	12	92	87
Run-4	24	86	81
Run-5	36	86	87
Run-6	48	80	79
Run-7	48	72	69

6.3 Additional kinetic data.

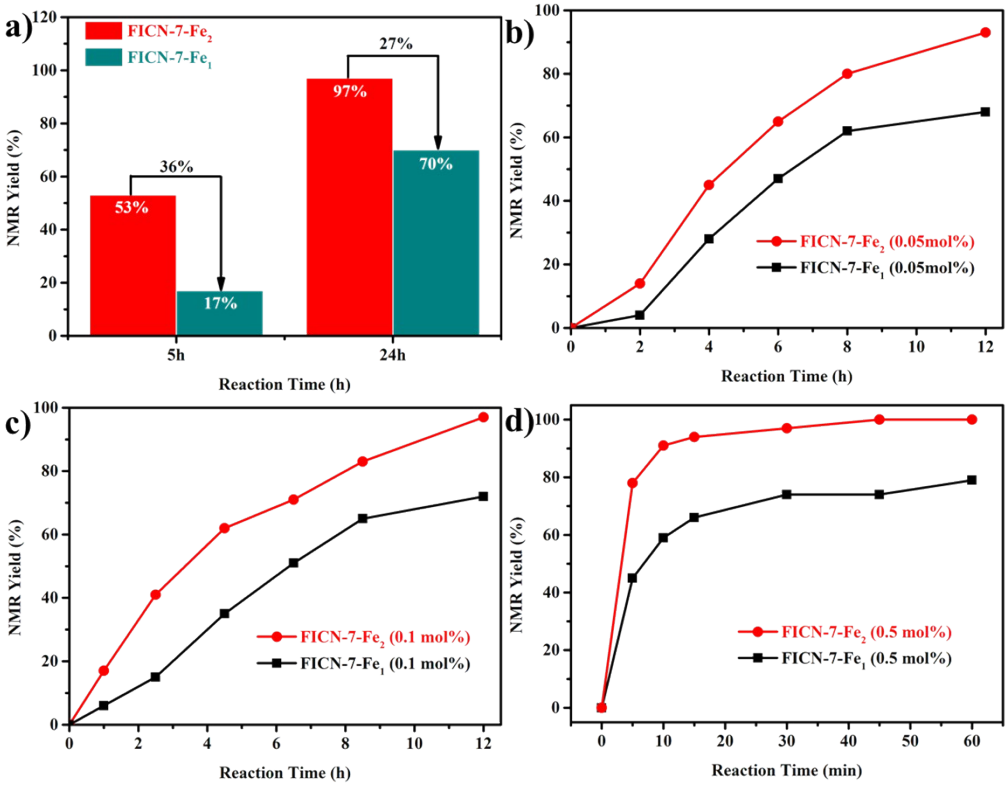

Figure S14. (a) Comparison of the yields obtained from the hydroboration of acetophenone with 0.05 mol% catalyst loading of FICN-7-Fe_2 and FICN-7-Fe_1 after different times. (b, c, d) Time-conversion curve of acetophenone hydroboration catalyzed by FICN-7-Fe_2 and FICN-7-Fe_1 at 0.05% Fe loading, 0.1% Fe loading, 0.5% Fe loading.

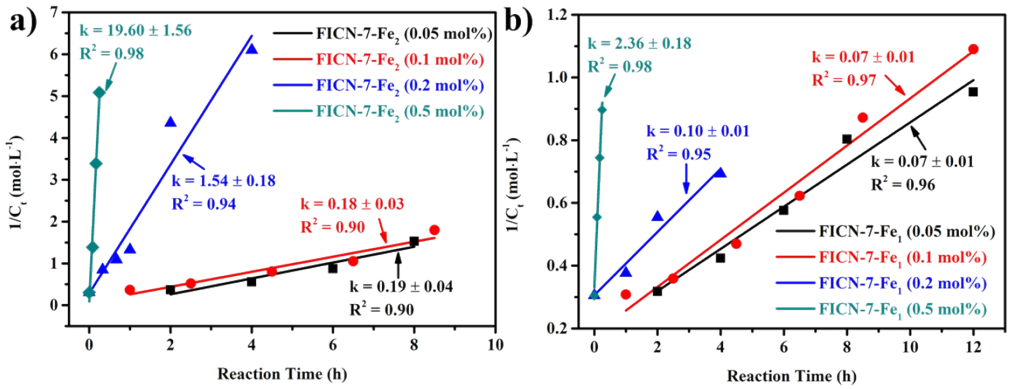

Figure S15. kinetic plots of acetophenone hydroboration catalyzed by FICN-7-Fe_2 (a) and FICN-7-Fe_1 (b) showing the pseudo-second order rate laws.

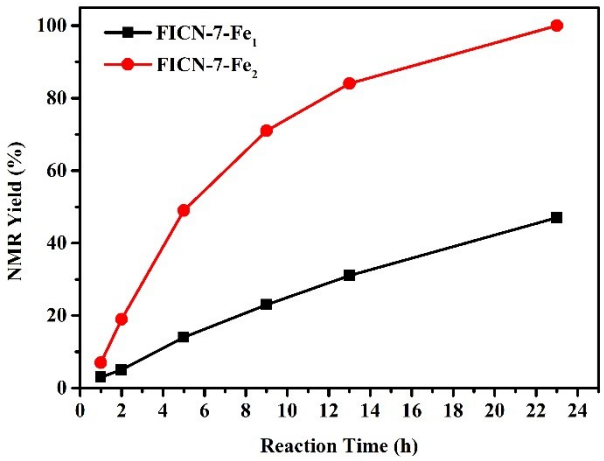

Figure S16. Time-conversion curve of acetophenone hydroboration catalyzed by FICN-7-Fe_2 and FICN-7-Fe_1 at 0.2% Fe loading and 10 equiv. of HBpin.

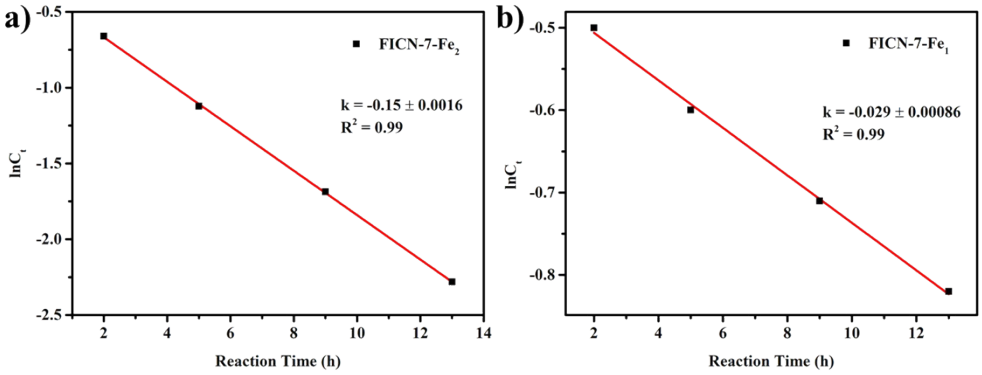

Figure S17. Kinetic plots of acetophenone hydroboration catalyzed by FICN-7-Fe_2 (a) and FICN-7-Fe_1 (b) with 10 equiv. of HBpin showing the first order rate laws.

6.4 Post-catalysis characterization.

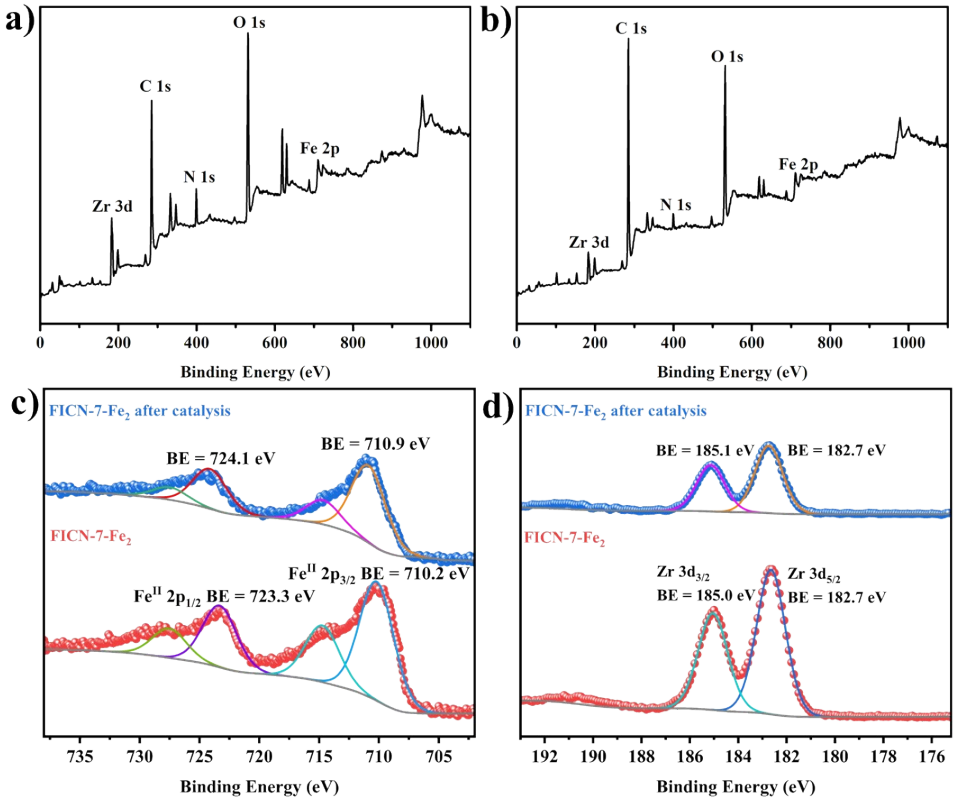

Figure S18. XPS data of FICN-7-Fe_2 and FICN-7-Fe_2 after catalysis.

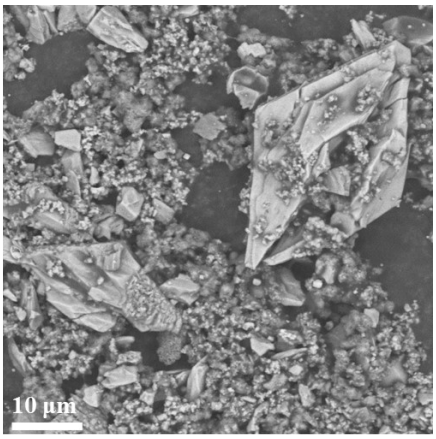

Figure S19. SEM images of FICN-7-Fe_2 after catalysis.

6.5 NMR spectra of catalysis products.

1-Phenylethanol (3a)[5] was isolated as colorless oil. Yield: 908.7 mg (93%). ^{1}H NMR (400 MHz, $CDCl_3$) δ 7.30 (d, J = 4.3 Hz, 4H), 7.23 (dq, J = 8.8, 4.3 Hz, 1H), 4.79 (q, J = 6.5 Hz, 1H), 2.65 (s, 1H), 1.42 (d, J = 6.5 Hz, 3H). ^{13}C NMR (101 MHz, $CDCl_3$) δ 145.90, 128.47, 127.41, 125.45, 70.28, 25.17.

1-(4-Methylphenyl)ethanol (3b)[5] was isolated as colorless oil. Yield: 672.2 mg (62%). ^{1}H NMR (400 MHz, $CDCl_3$) δ 7.19 (d, J = 8.0 Hz, 2H), 7.10 (d, J = 7.8 Hz, 2H), 4.74 (q, J = 6.4 Hz, 1H), 2.30 (d, J = 6.8 Hz, 3H), 1.39 (d, J = 6.5 Hz, 3H). ^{13}C NMR (101 MHz, $CDCl_3$) δ 142.98, 136.90, 129.07, 125.39, 70.01, 25.08, 21.09.

1-(4-Methoxyphenyl)ethanol (3c)[6] was isolated as colorless oil. Yield: 652.6 mg (54%). ^{1}H NMR (400 MHz, $CDCl_3$) δ 7.23 (d, J = 8.5 Hz, 2H), 6.83 (d, J = 8.7 Hz, 2H), 4.76 (q, J = 6.2 Hz, 1H), 3.75 (s, 3H), 2.70 (s, 1H), 1.41 (d, J = 6.5 Hz, 3H). ^{13}C NMR (101 MHz, $CDCl_3$) δ 158.79, 138.13, 126.68, 113.73, 69.73, 55.23, 25.03.

1-(4-nitrophenyl)ethanol (3d)[7] was isolated as yellow oil. Yield: 1.280 g (96%). ^{1}H NMR (400 MHz, $CDCl_3$) δ 8.05 (d, J = 7.5 Hz, 2H), 7.45 (d, J = 8.0 Hz, 2H), 4.92 (q, J = 6.2 Hz, 1H), 3.51 (s, 1H), 1.42 (d, J = 6.4 Hz, 3H). ^{13}C NMR (101 MHz, $CDCl_3$) δ 153.44, 146.79, 126.10, 123.55, 69.20, 25.25.

Diphenylmethanol (3f)[5] was isolated as White solid. Yield: 866.6 mg (59%). ^{1}H NMR (400 MHz, Chloroform-d) δ 7.38 (q, J = 7.5 Hz, 8H), 7.33 – 7.27 (m, 2H), 5.80 (s, 1H), 2.66 (s, 1H). ^{13}C NMR (101 MHz, Chloroform-d) δ 143.86, 128.54, 127.60, 126.63,

76.22.

Benzyl Alcohol (3i)[6] was isolated as colorless oil. Yield: 692.7 mg (80%). ^{1}H NMR (400 MHz, $CDCl_3$) δ 7.35 (dq, J = 12.1, 6.5, 5.7 Hz, 5H), 4.59 (s, 2H), 3.29 (s, 1H). ^{13}C NMR (101 MHz, $CDCl_3$) δ 140.86, 128.46, 127.48, 126.99, 64.86.

4-Methyl benzyl alcohol (3j)[6] was isolated as White solid. Yield: 906.0 mg (93%). ^{1}H NMR (400 MHz, $CDCl_3$) δ 7.22 (d, J = 7.6 Hz, 2H), 7.15 (d, J = 7.7 Hz, 2H), 4.59 (s, 2H), 2.34 (s, 3H), 2.06 (s, 1H). ^{13}C NMR (101 MHz, $CDCl_3$) δ 137.99, 137.42, 129.30, 127.21, 65.22, 21.24.

4-Chloride benzyl alcohol (3k)[6] was isolated as White solid. Yield: 987.6 mg (87%). ^{1}H NMR (400 MHz, $CDCl_3$) δ 7.31 (q, J = 8.5 Hz, 4H), 4.67 (s, 2H), 1.73 (s, 1H).^{13}C NMR (101 MHz, $CDCl_3$) δ 139.28, 133.35, 128.71, 128.34, 64.42.

Diphenylmethanamine (3l)[8] was isolated as yellow oil. Yield: 624.5 mg (85%). ^{1}H NMR (400 MHz, $CDCl_3$) δ 7.31 (d, J = 7.3 Hz, 4H), 7.24 (t, J = 7.5 Hz, 4H), 7.16 (t, J = 7.2 Hz, 2H), 5.10 (s, 1H), 1.91 (s, 2H). ^{13}C NMR (101 MHz, $CDCl_3$) δ 145.47, 128.38, 126.85, 126.82, 59.60.

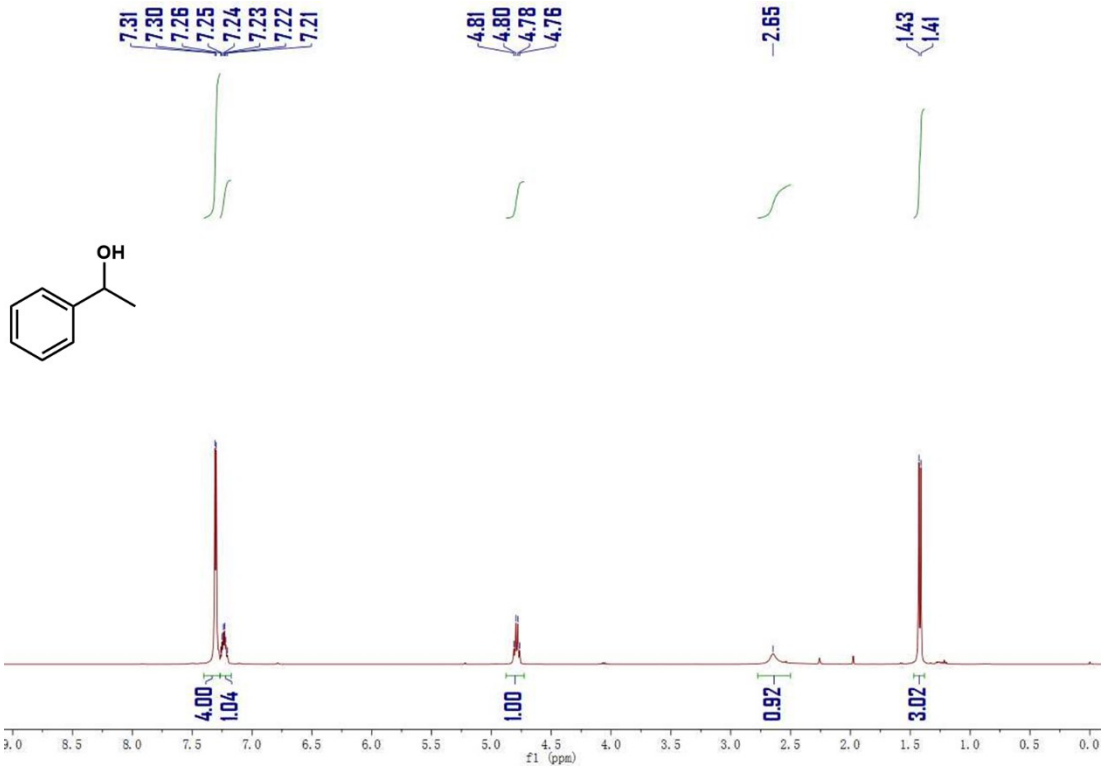

Figure S20. ^{1}H NMR (400 MHz, $CDCl_3$) spectrum of 1-phenylethanol (3a).

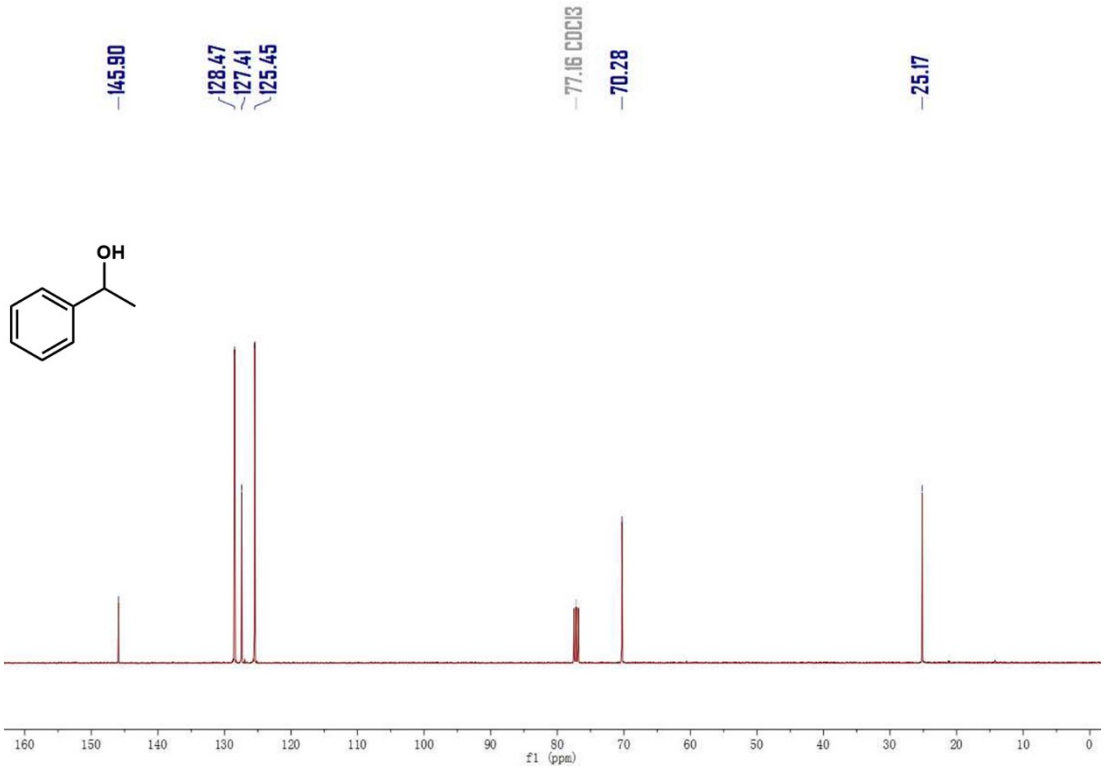

Figure S21. ^{13}C NMR (101 MHz, CDCl3) spectrum of 1-phenylethanol (3a).

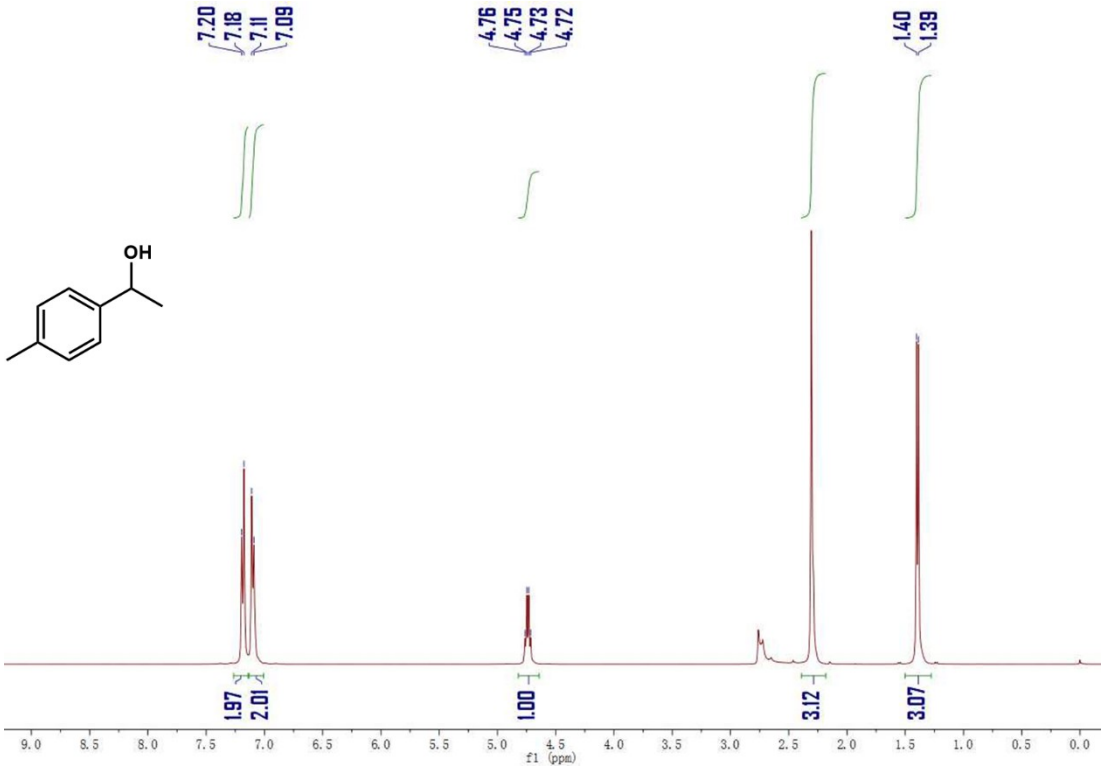

Figure S22. ^{1}H NMR (400 MHz, $CDCl_3$) spectrum of 1-(4-methylphenyl)ethanol (3b).

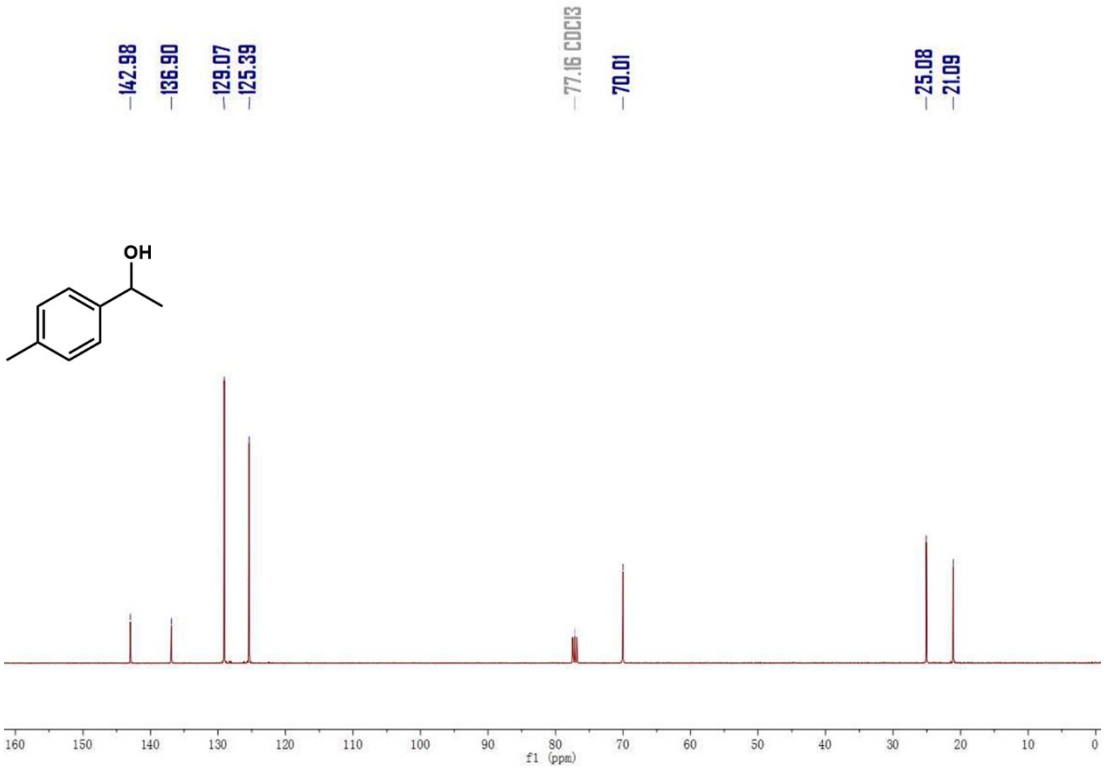

Figure S23. ^{13}C NMR (101 MHz, $CDCl_3$) spectrum of 1-(4-methylphenyl)ethanol (3b).

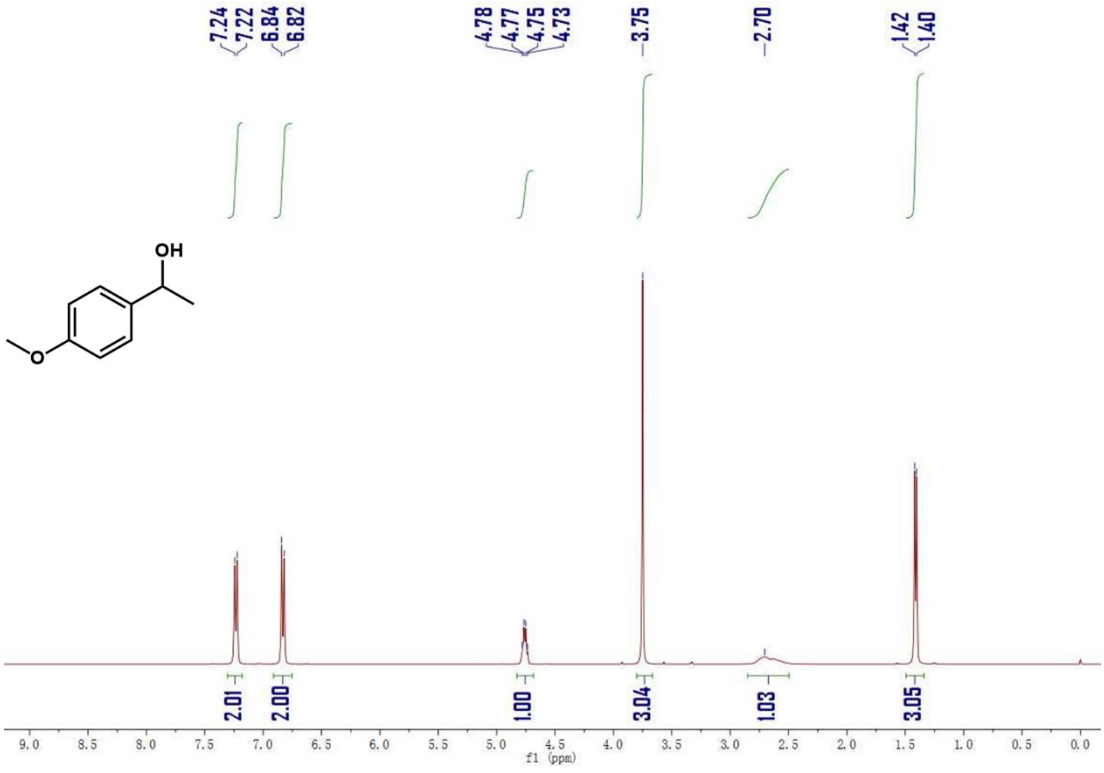

Figure S24. ^{1}H NMR (400 MHz, $CDCl_3$) spectrum of 1-(4-methoxyphenyl)ethanol (3c).

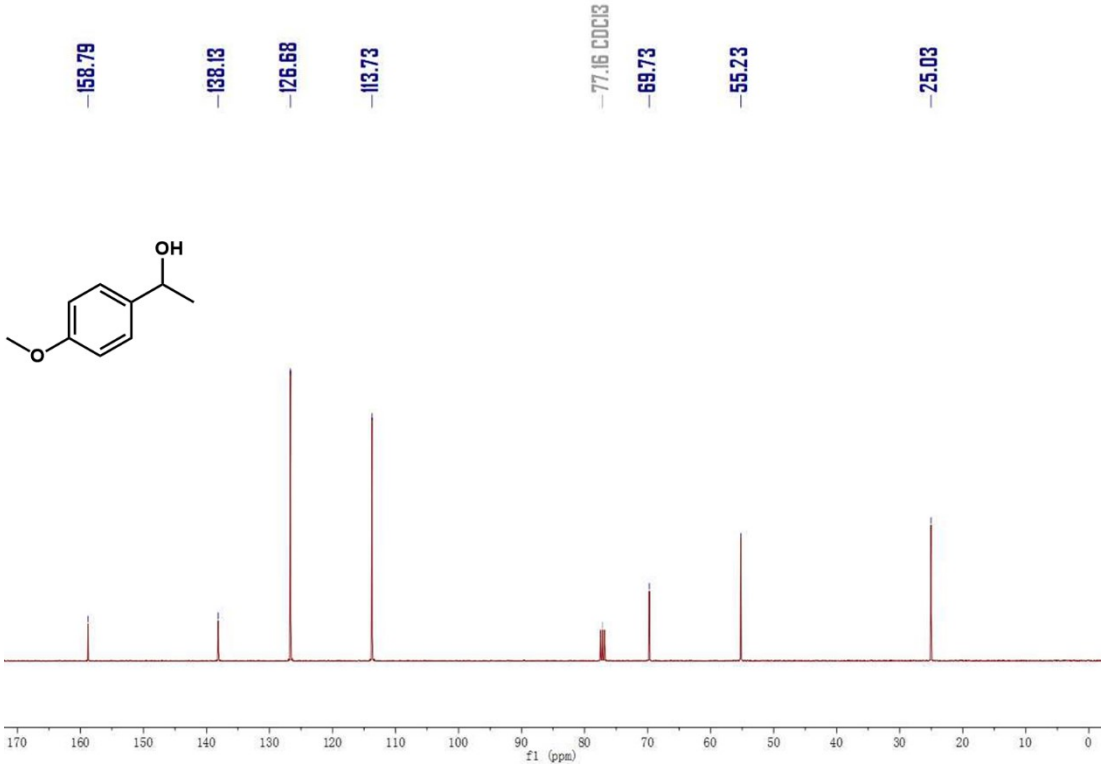

Figure S25. ^{13}C NMR (101 MHz, $CDCl_3$) spectrum of 1-(4-methoxyphenyl)ethanol (3c).

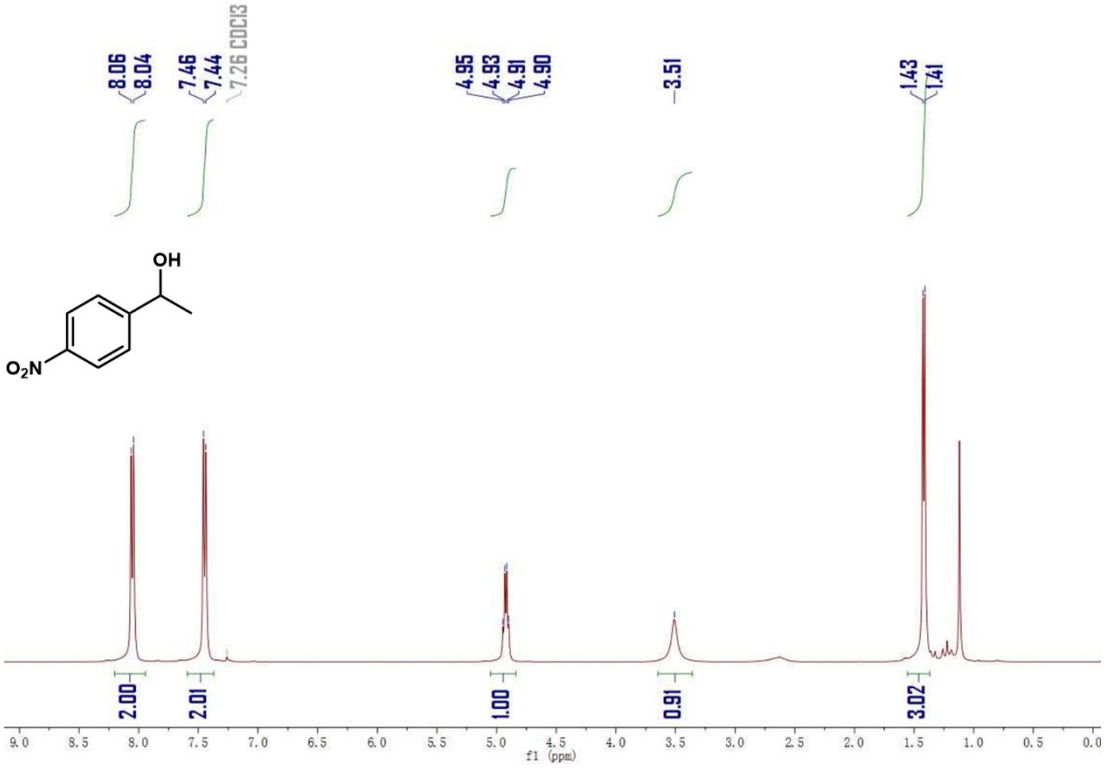

Figure S26. ^{1}H NMR (400 MHz, $CDCl_3$) spectrum of 1-(4-nitrophenyl)ethanol (3d).

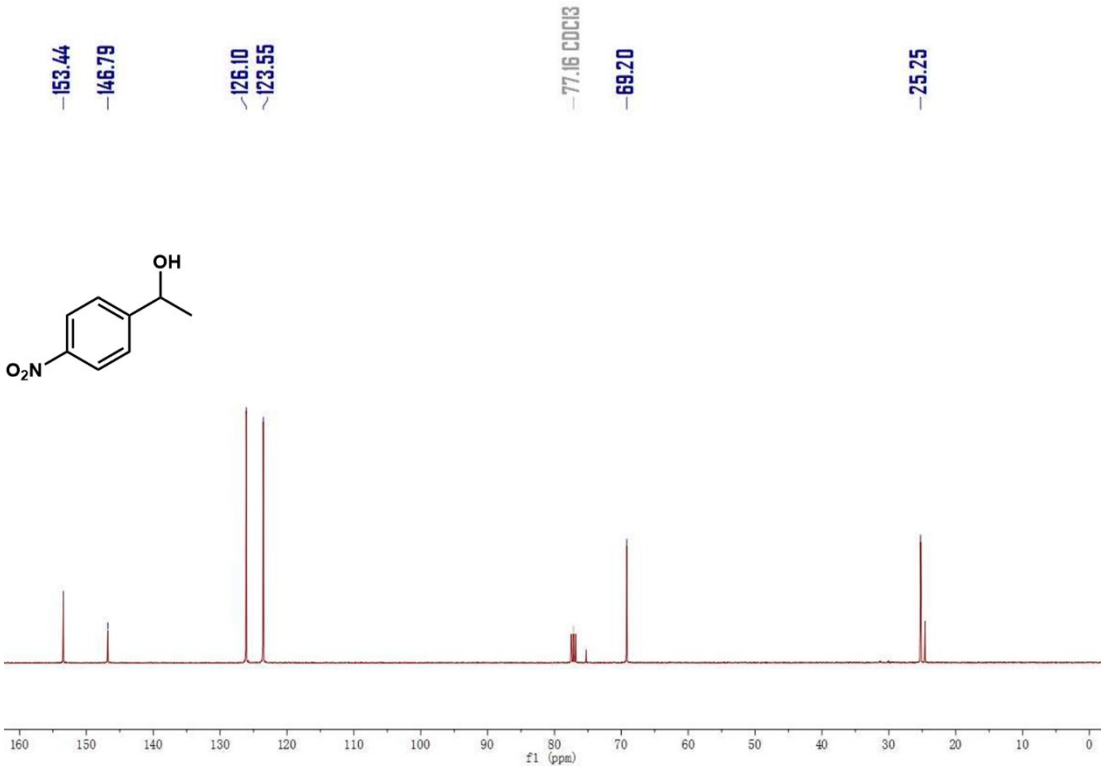

Figure S27. ^{13}C NMR (101 MHz, $CDCl_3$) spectrum of 1-(4-nitrophenyl)ethanol (3d).

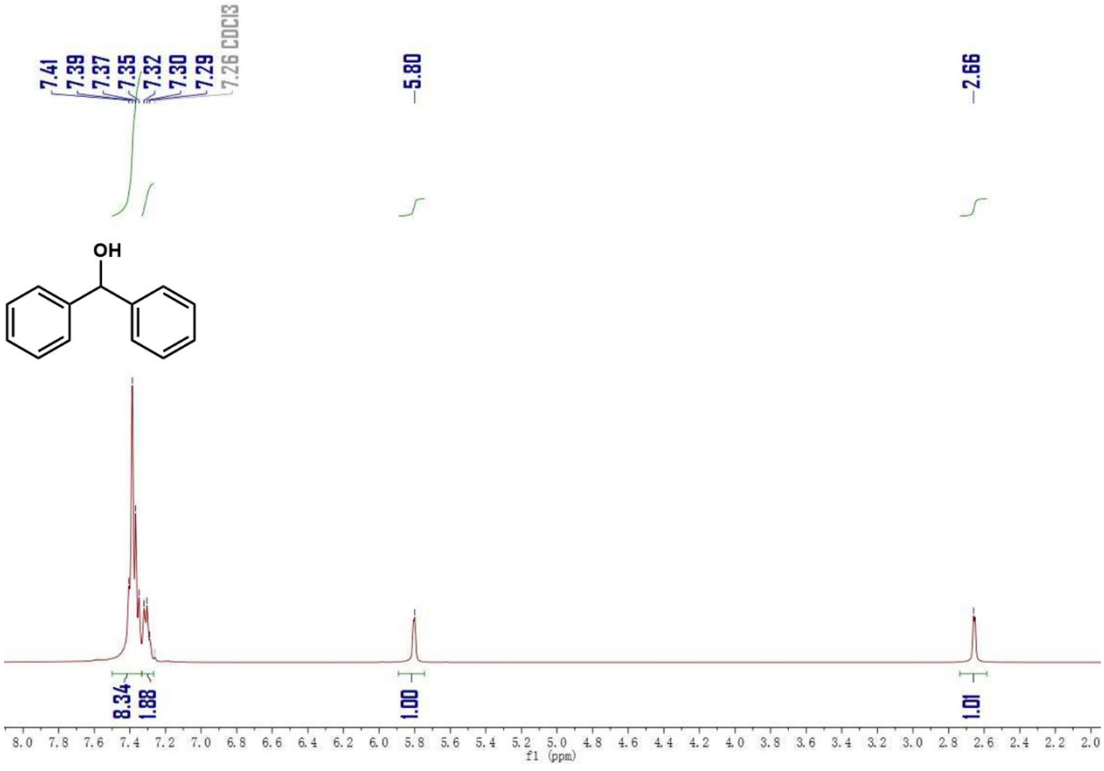

Figure S28. ^{1}H NMR (400 MHz, $CDCl_3$) spectrum of Diphenylmethanol (3f).

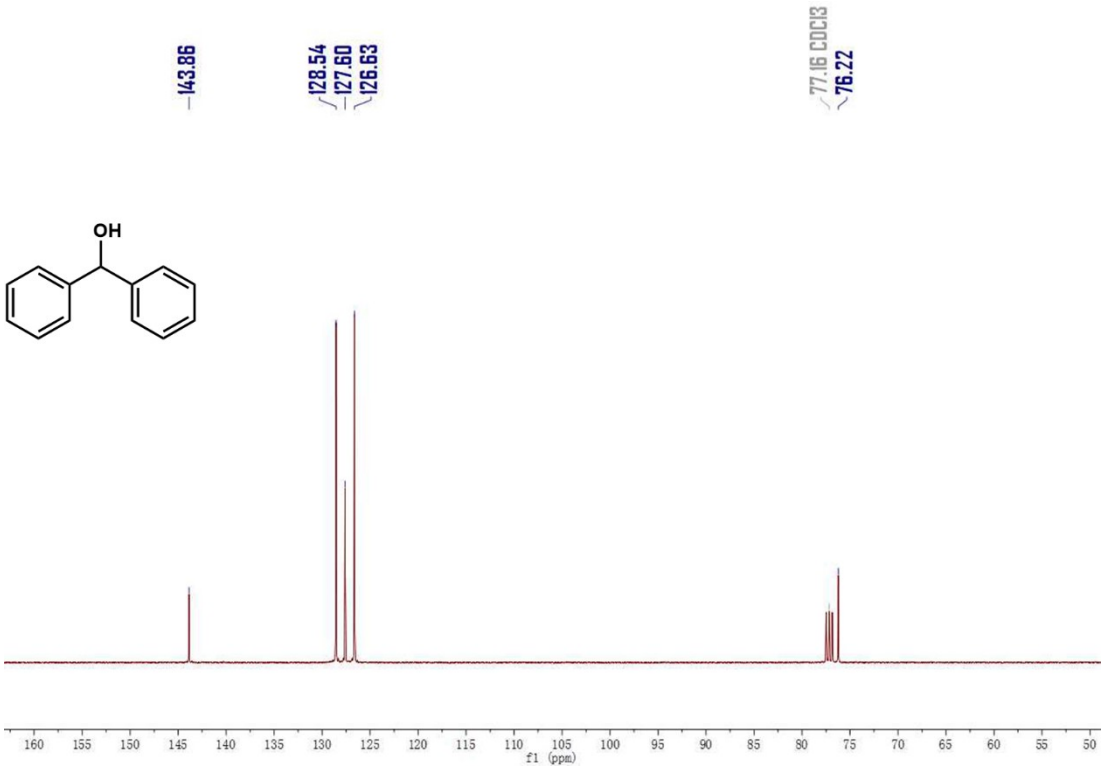

Figure S29. ^{13}C NMR (101 MHz, $CDCl_3$) spectrum of Diphenylmethanol (3f).

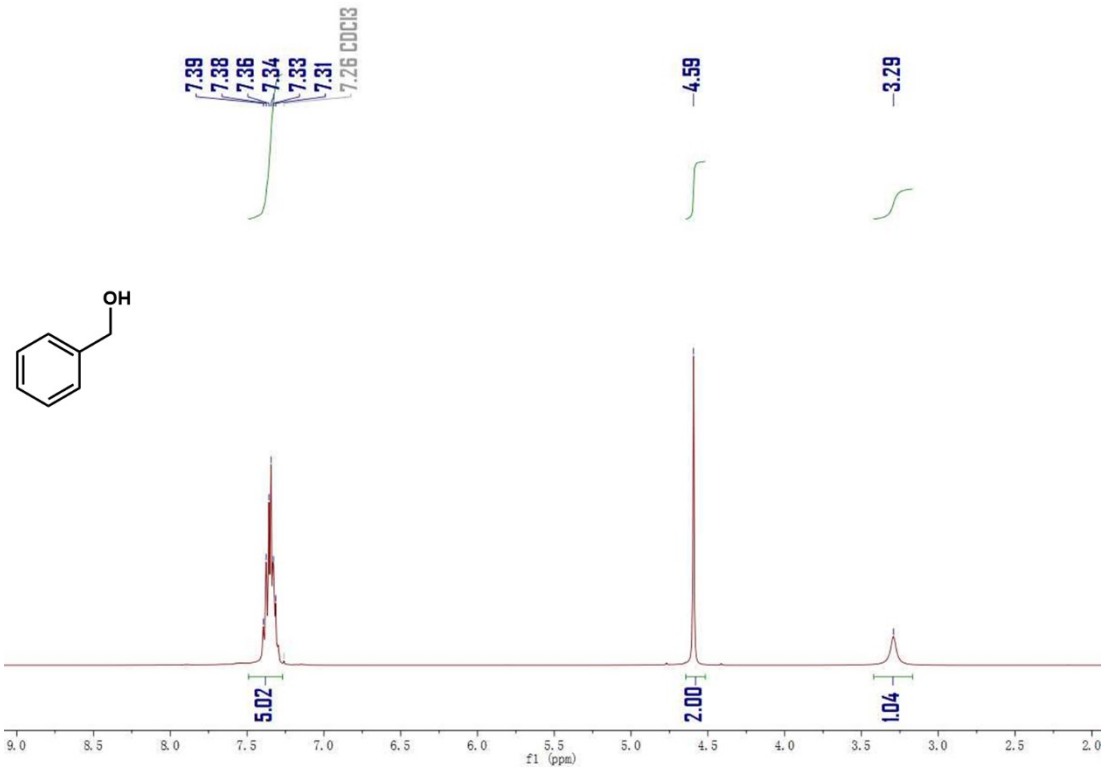

Figure S30. ^{1}H NMR (400 MHz, $CDCl_3$) spectrum of benzyl Alcohol (3i).

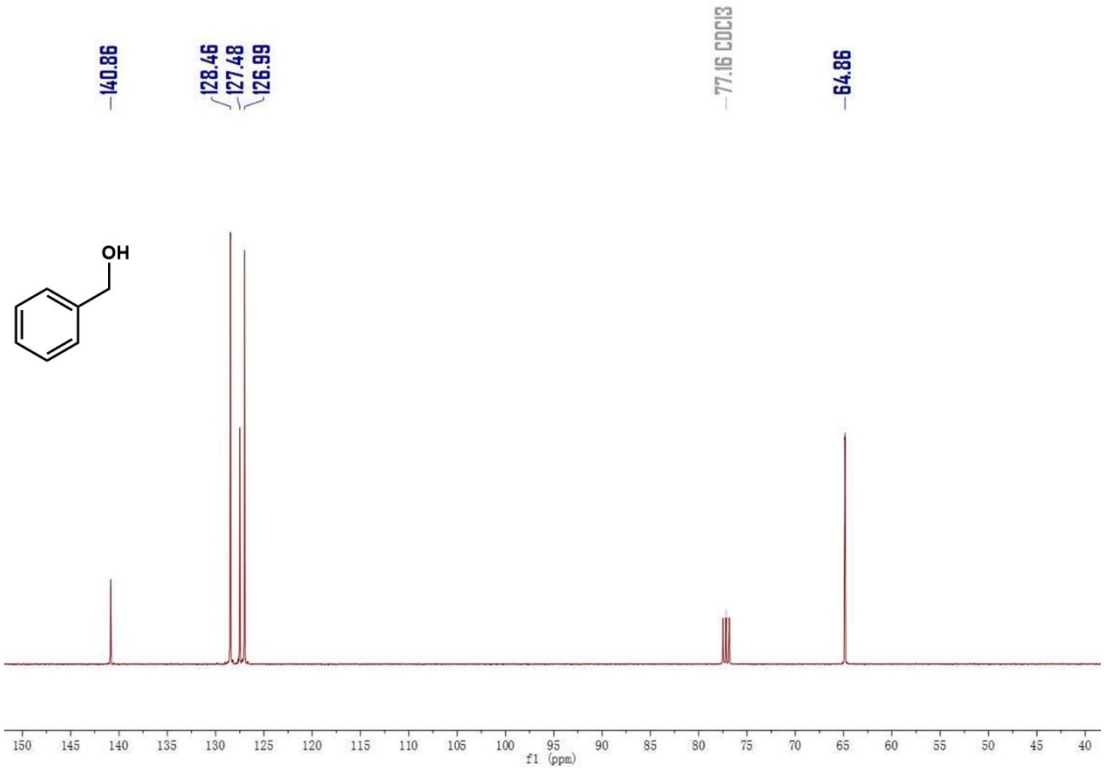

Figure S31. ^{13}C NMR (101 MHz, $CDCl_3$) spectrum of benzyl Alcohol (3i).

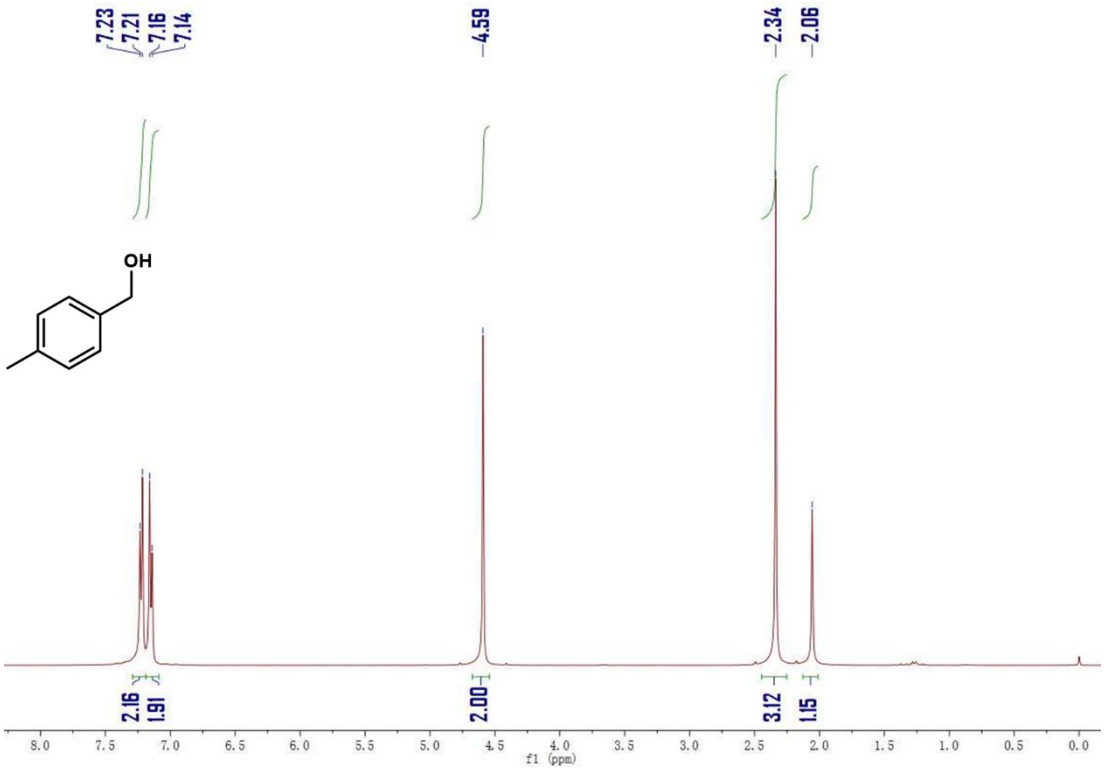

Figure S32. ^{1}H NMR (400 MHz, $CDCl_3$) spectrum of 4-methyl benzyl alcohol (3j).

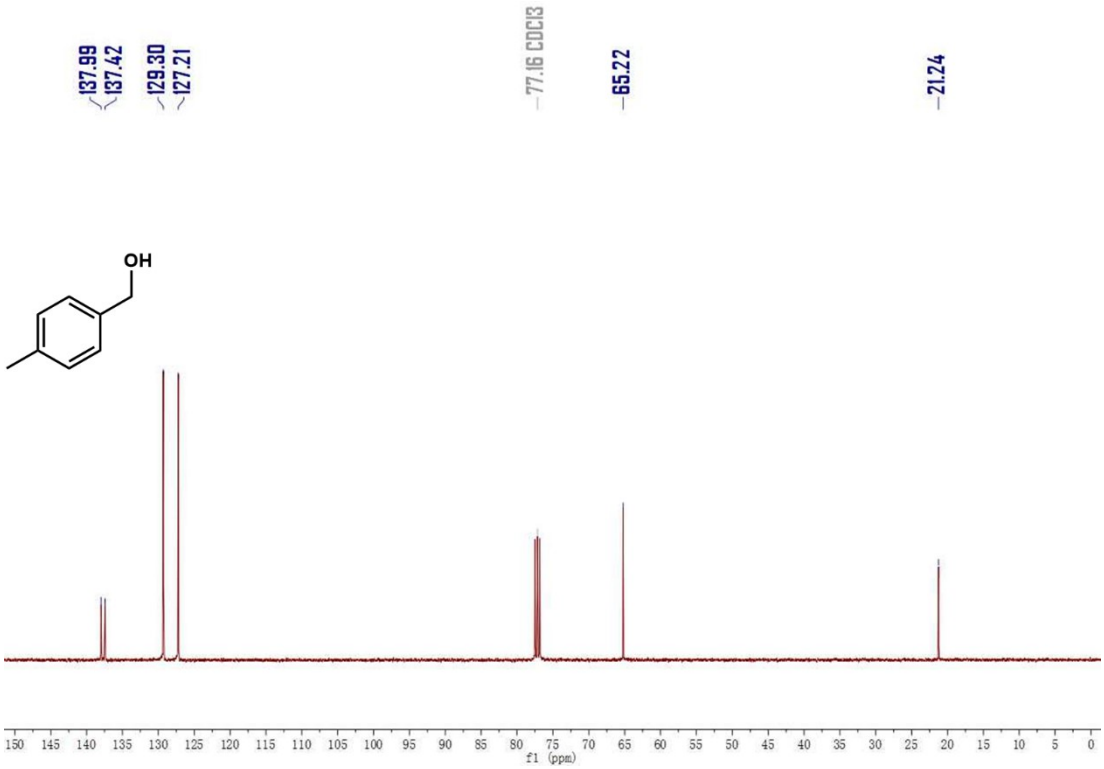

Figure S33. ^{13}C NMR (101 MHz, $CDCl_3$) spectrum of 4-methyl benzyl alcohol (3j).

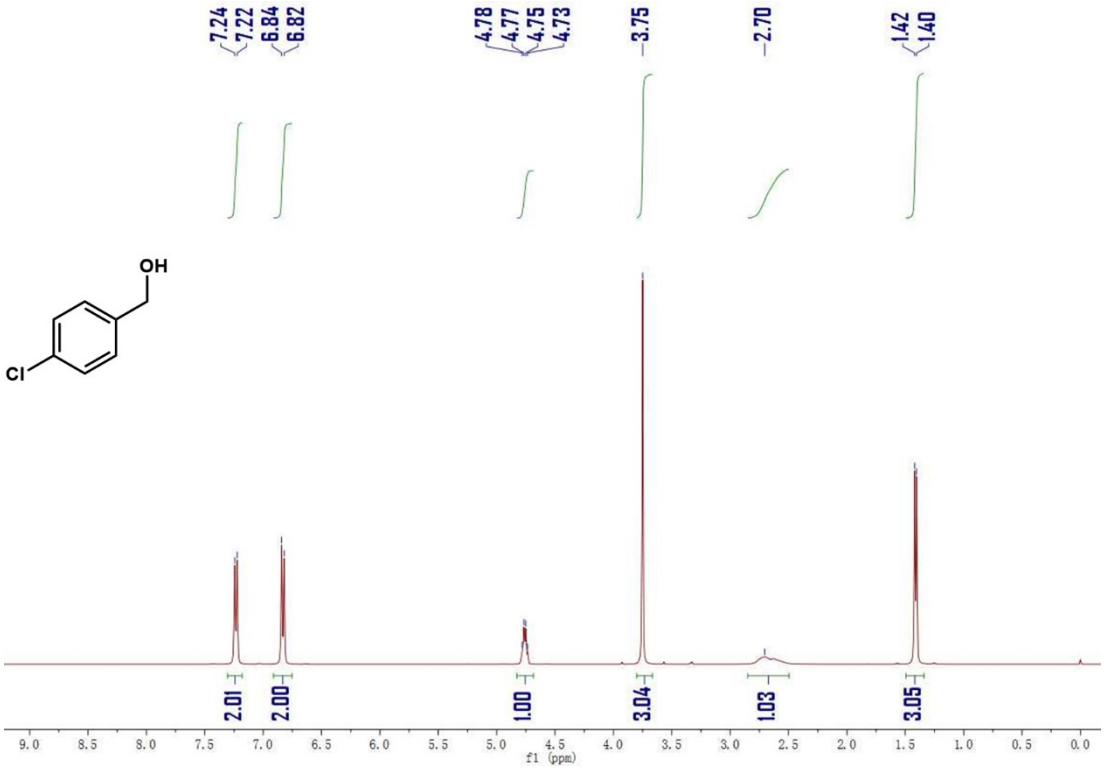

Figure S34. ^{1}H NMR (400 MHz, $CDCl_3$) spectrum of 4-chloride benzyl alcohol (3k).

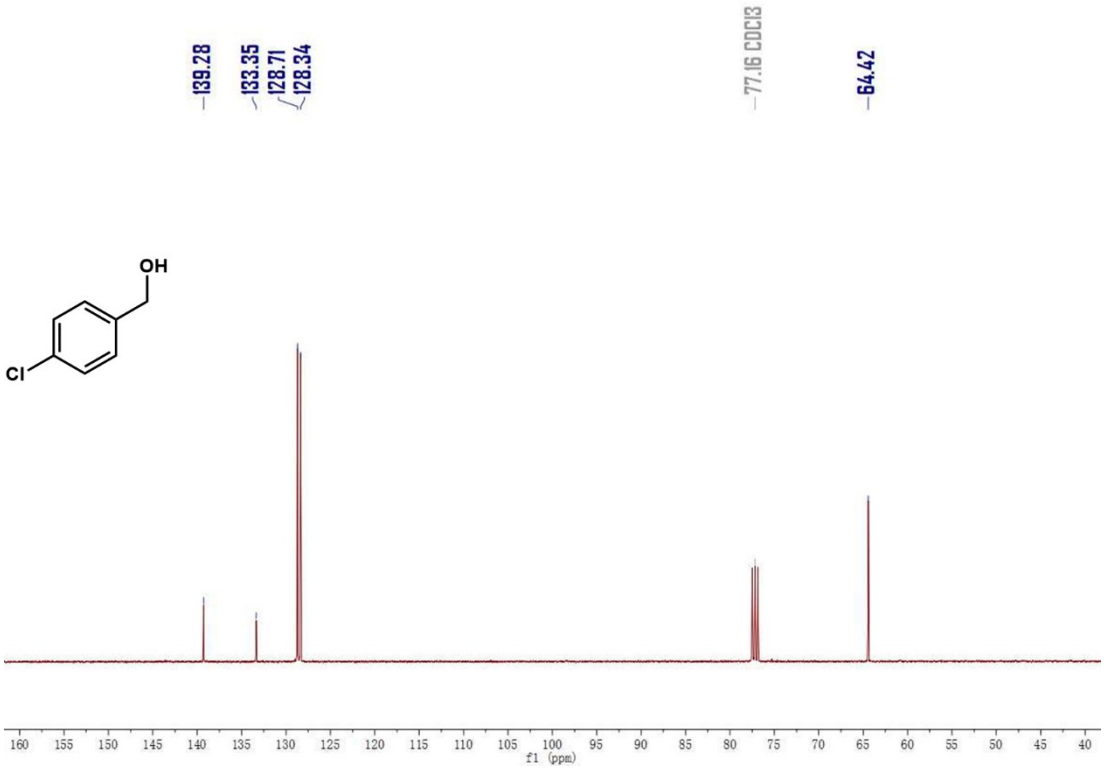

Figure S35. ^{13}C NMR (101 MHz, $CDCl_3$) spectrum of 4-chloride benzyl alcohol (3k).

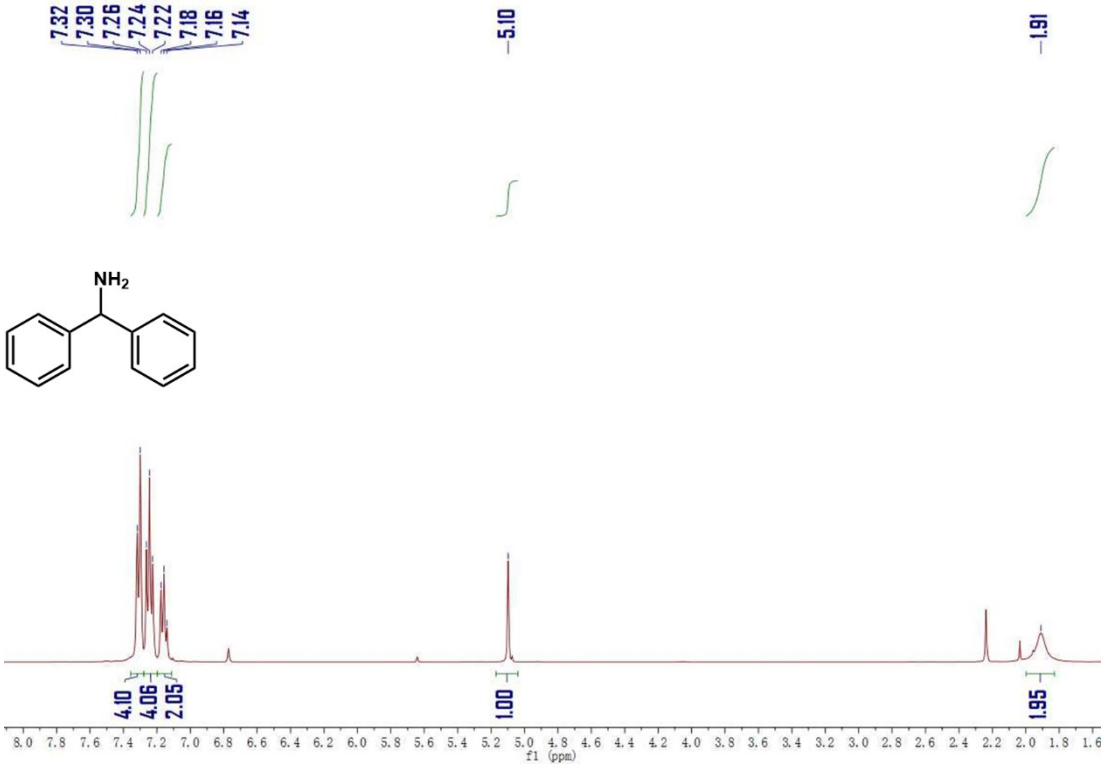

Figure S36. ^{1}H NMR (400 MHz, $CDCl_3$) spectrum of diphenylmethanamine (3l).

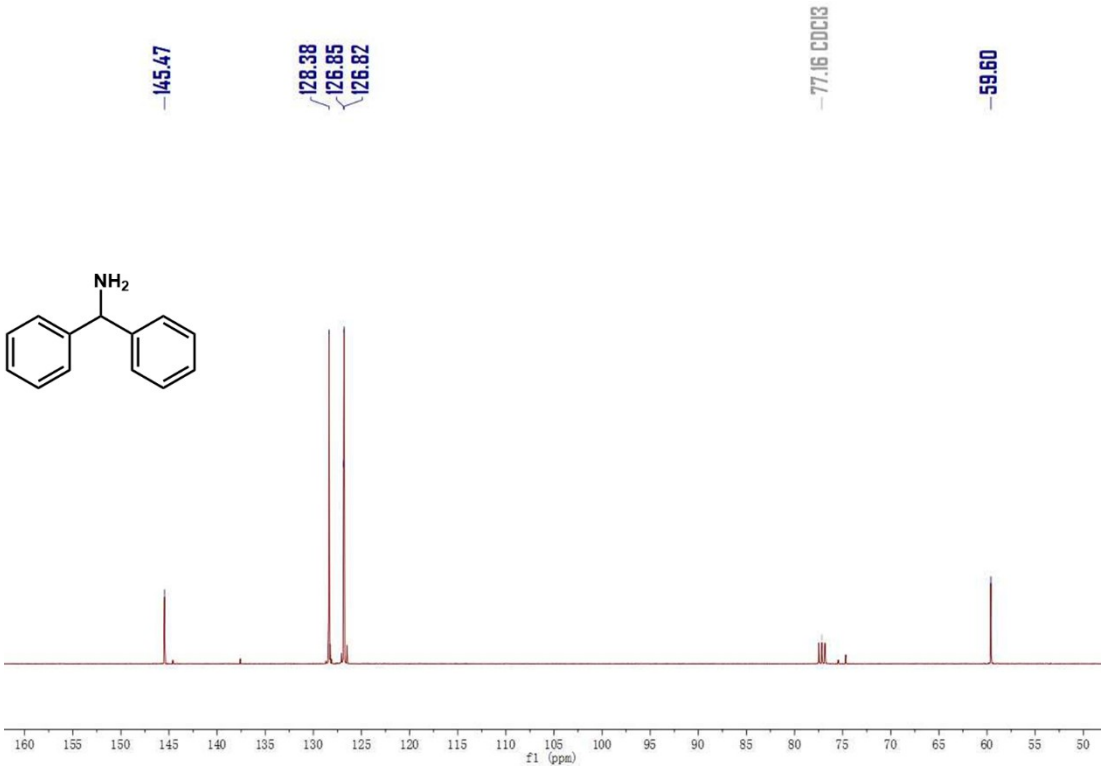

Figure S37. ^{13}C NMR (101 MHz, $CDCl_3$) spectrum of diphenylmethanamine (3l).

7. Activity Comparison of FICN-7-Fe_2 with reported Fe catalysts

Table S6. Selected examples of reported Fe catalysts for hydroboration of acetophenone.

Entry	Catalyst	Reaction conditions	Substrate dosage	Yield (%)	reference
1	$Fe(acac)_3$ complex	10 mol% cat., 10 mol%$NaBEt_3H$, THF	Ketone (1.0 mmol) HBpin (1.5 mmol)	62	5
2	$Fe_2(NPtBu_3)_4$ complex	2.5mol% cat., benzene	Ketone (0.2 mmol) HBpin (0.22 mmol)	65	9
3	Fe_2O_3-nanoparticle	5mol% cat., Toluene	Ketone (0.25 mmol) HBpin (0.3 mmol)	82	6

4	Iron (II) coordination polymer	0.1 mol% cat., 2 mol% KO^{t}Bu, THF	Ketone (1 mmol) HBpin (1.1 mmol)	98	[10]
5	[Fe−N_2S_2]$_2$ complex	0.1 mol%cat., benzene	Aldehyde (0.436 mmol) HBpin (0.436 mmol)	99	[11]
6	[Fe{N(SiMe$_3$)$_2$}$_2$] complex	3 mol% cat., THF	Ketone (0.25 mmol) HBpin (0.3 mmol)	99	[12]
7	[LSi(FeBr$_2$·THF)]$_2$ complex	10 mol% cat., MeCN	Ketone (0.1 mmol) HBpin (0.15 mmol)	97	[13]
8	Iron (II) coordination polymer	0.1 mol% cat., 2 mol% KO^{t}Bu, neat	Ketone (1 mmol) HBpin (1.1 mmol)	98	[7]
9	Bis (NHSi) hydrido Fe (II) complex	1 mol% cat., THF	Ketone (1 mmol) HBpin (1.1 mmol)	99	[14]
10	1-[K([18]c-6)(thf)$_{0.5}$]	0.1 mol% cat., THF	Ketone (1 mmol) HBpin (1.03 mmol)	99	[15]
11	L-valim-UiO-Fe	0.5 mol% cat., THF	Ketone (0.14 mmol) HBpin (0.17 mmol)	99	[16]
12	Vol-UiO-Fe	0.05 mol% cat., THF	Ketone (0.585 mmol) HBpin (0.643 mmol)	98	[17]
13	FICN-Fe$_2$(Cl)	0.05 mol% cat., neat	Ketone (8 mmol) HBpin (10.4 mmol)	97	This work

8. References

1. Sheldrick, G. M., Crystal structure refinement with SHELXL. *Acta Crystallogr C Struct Chem* **2015,** *71* (Pt 1), 3-8.
2. Spek, A. L., PLATON SQUEEZE: a tool for the calculation of the disordered solvent contribution to the calculated structure factors. *Acta Crystallogr C Struct Chem* **2015,** *71* (Pt 1), 9-18.
3. Ravel, B.; Newville, M., ATHENA, ARTEMIS, HEPHAESTUS: data analysis for X-ray absorption spectroscopy using IFEFFIT. *Journal of Synchrotron Radiation* **2005,** *12* (4), 537-541.
4. Rehr, J. J.; Albers, R. C., Theoretical approaches to x-ray absorption fine structure. *Reviews of Modern Physics* **2000,** *72* (3), 621-654.
5. Tamang, S. R.; Findlater, M., Iron Catalyzed Hydroboration of Aldehydes and Ketones. *J Org Chem* **2017,** *82* (23), 12857-12862.
6. Shegavi, M. L.; Baishya, A.; Geetharani, K.; Bose, S. K., Reusable Fe2O3-nanoparticle catalysed efficient and selective hydroboration of carbonyl compounds. *Organic Chemistry Frontiers* **2018,** *5* (24), 3520-3525.
7. Zhang, G.; Cheng, J.; Davis, K.; Bonifacio, M. G.; Zajaczkowski, C., Practical and selective hydroboration of aldehydes and ketones in air catalysed by an iron(ii) coordination polymer. *Green Chemistry* **2019,** *21* (5), 1114-1121.
8. Yan, D.; Wu, X.; Xiao, J.; Zhu, Z.; Xu, X.; Bao, X.; Yao, Y.; Shen, Q.; Xue, M., n-Butyllithium catalyzed hydroboration of imines and alkynes. *Organic Chemistry Frontiers* **2019,** *6* (5), 648-653.
9. Bai, T.; Janes, T.; Song, D., Homoleptic iron(ii) and cobalt(ii) bis(phosphoranimide) complexes for the selective hydrofunctionalization of unsaturated molecules. *Dalton Trans* **2017,** *46* (37), 12408-12412.
10. Li, L.; Liu, E.; Cheng, J.; Zhang, G., Iron(ii) coordination polymer catalysed hydroboration of ketones. *Dalton Trans* **2018,** *47* (29), 9579-9584.
11. Das, U. K.; Higman, C. S.; Gabidullin, B.; Hein, J. E.; Baker, R. T., Efficient and Selective Iron-Complex-Catalyzed Hydroboration of Aldehydes. *ACS Catalysis* **2018,** *8* (2), 1076-1081.
12. Baishya, A.; Baruah, S.; Geetharani, K., Efficient hydroboration of carbonyls by an iron(ii) amide catalyst. *Dalton Trans* **2018,** *47* (28), 9231-9236.
13. Khoo, S.; Cao, J.; Ng, F.; So, C. W., Synthesis of a Base-Stabilized Silicon(I)-Iron(II) Complex for Hydroboration of Carbonyl Compounds. *Inorg Chem* **2018,** *57* (20), 12452-12455.
14. Qi, X.; Zheng, T.; Zhou, J.; Dong, Y.; Zuo, X.; Li, X.; Sun, H.; Fuhr, O.; Fenske, D., Synthesis and Catalytic Activity of Iron Hydride Ligated with Bidentate N-Heterocyclic Silylenes for Hydroboration of Carbonyl Compounds. *Organometallics* **2019,** *38* (2), 268-277.
15. Maier, T. M.; Gawron, M.; Coburger, P.; Bodensteiner, M.; Wolf, R.; van Leest, N. P.; de Bruin, B.; Demeshko, S.; Meyer, F., Low-Valence Anionic alpha-Diimine Iron Complexes: Synthesis, Characterization, and Catalytic Hydroboration Studies.

Inorg Chem **2020,** *59* (21), 16035-16052.
16. Newar, R.; Akhtar, N.; Antil, N.; Kumar, A.; Shukla, S.; Begum, W.; Manna, K., Amino Acid-Functionalized Metal-Organic Frameworks for Asymmetric Base-Metal Catalysis. *Angew Chem Int Ed Engl* **2021,** *60* (19), 10964-10970.
17. Antil, N.; Akhtar, N.; Newar, R.; Begum, W.; Kumar, A.; Chauhan, M.; Manna, K., Chiral Iron(II)-Catalysts within Valinol-Grafted Metal–Organic Frameworks for Enantioselective Reduction of Ketones. *ACS Catalysis* **2021,** *11* (16), 10450-10459.